Multiple phase rifting and subsequent inversion in the West Netherlands Basin: implications for geothermal reservoir characterization

Annelotte Weert[1], Kei Ogata[1], Francesco Vinci[2], Coen Leo[3], Giovanni Bertotti[4], Jerome Amory[2], Stefano Tavani[1,5]

[1]Department of Earth, Environmental and Resource Sciences (DiSTAR), University of Naples 'Federico II', Naples, 80126, Italy
[2]PanTerra Geoconsultants B.V., Leiderdorp, 2352BZ, The Netherlands
[3]Geoleo B.V. Consultancy, The Hague, 2596PL, The Netherlands
[4]Faculty of Civil Engineering and Geosciences, Technical University of Delft, Delft, 2628CN, The Netherlands
[5]Consiglio Nazionale delle Ricerche, IGAG, Rome, 00185, Italy

Correspondence to: Annelotte Weert (annelotteweert@gmail.com)

Abstract. Aiming to contribute to the energy transition, this study provides an integrated picture of the geothermal system hosted in the West Netherlands Basin and shows how the reconstruction of the basin's geological history can contribute to the correct exploration~~itation~~ and exploitation of its geothermal resources. In the West Netherlands Basin, the main geothermal targets are found in the Cretaceous and Jurassic strata that were deposited during the rifting and post-rifting stages and were deformed during the subsequent basin inversion. Despite multiple studies on the tectonic setting, the timing and tectono-stratigraphic architecture of the rift system and its overall control on the development and evolution of geothermal systems are still to be fully deciphered. A~~In this framework, a~~ detailed interpretation of the syn- and post-rift intervals in the West Netherlands Basin will be given within the framework of geothermal exploration~~,~~ using ~~With a renewed interpretation of~~ a recently released and reprocessed seismic 3D cube, which covers~~ing~~ a large portion of the onshore section of the basin~~,~~ ~~w~~We identified two major~~important~~ Jurassic rifting episodes and one Late Cretaceous inversion event. During the~~These two~~ Jurassic rifting phases the compartmentalisation of the basin and creation of ~~not only created sedimentary~~ accommodation space~~, but also caused compartmentalisation of the depocenters~~ let to the deposition of the Late Jurassic Nieuwerkerk Formation, which is the main regional producing geothermal target. ~~Accordingly,~~ Within this formation, we individuate growth synclines located in the central portions of the Jurassic half-grabens ~~show~~as sites that show good potential for geothermal exploration.

1 Introduction

Subsurface fluid flow systems hosted in rift basins form part of the resources that are indispensable in the global challenge to cut greenhouse gas emissions and cover current and future needs with sustainable energy sources. Basins' bounding faults and the laterally and vertically varying petrological characteristics of their ~~sedimentary basins'~~ infill~~s~~, control the distribution, abundance and recoverability of these resources (Gawthorpe and Leeder, 2000). This~~,~~ includes~~ing~~ the heat flow needed for

high (T > 150°C) to low (T < 90°C) enthalpy geothermal systems (Carapezza et al., 2022). As a frontrunner in Europe, the Netherlands recognizes the contribution of geothermal energy to be crucial for a successful energy transition (e.g. Kramers et al., 2012; Willems and Nick, 2019; Mijnlieff, 2020).

The West Netherlands Basin (WNB) (Fig. 1~~a~~) is a former prosperous hydrocarbon province where the interest changed to geothermal energy in the past decade. Having an energy-demanding greenhouse horticulture, a dense population, which includes the cities of Rotterdam and The Hague, and an average geothermal gradient of 31°C km^{-1} (Bonté et al., 2012), the WNB is considered as one of the best case studies for low-enthalpy geothermal exploration (Kramers et al., 2012; Crooijmans et al., 2016; Willems et al., 2017c; Willems, 2017; Vondrak et al., 2018; Willems and Nick, 2019; Willems et al., 2020; Boersma et al., 2021). A typical geothermal project in the Netherlands comprises a low-enthalpy geothermal system for direct heat that contains two or more wells; hot water is produced by production wells and re-injected by injection wells after the heat has been extracted (Limberger et al., 2018). In the WNB, only open loop geothermal systems (i.e. a geothermal doublet that uses the aquifer as heat exchanger) reaching production temperatures ranging from 70°C to 90°C are used (Willems et al., 2017b). For~~With the~~ hydrocarbon exploitation in the WNB, an extensive data collection was gathered (e.g. seismic and well data), which is publicly available at https://www.nlog.nl/datacenter/ ~~nlog.nl~~ (e.g. Duin et al., 2006; Kombrink et al., 2012). Up to 2023, 14 geothermal projects were realised in the area (Geothermie Nederland, 2023), targeting aquifers hosted by the post-rift Cretaceous Rijnland Group (two projects), the syn-rift Jurassic Nieuwerkerk Formation (ten projects), and the pre-rift Triassic Buntsandstein (two projects). Financial budgets for geothermal projects are much tighter than for traditional hydrocarbon exploration, making the successful delivery of every well essential to ensure the economic profitability of the geothermal projects. Understanding how the tectonic evolution of a rift basin influences the key parameters used for planning geothermal wells is therefore critical. Such parameters include aquifer thickness and heterogeneity (e.g. Poulsen et al., 2015). A thicker and more homogeneous reservoir ~~is preferred, as it~~ allows for better fluid flow, a higher heat extraction and an increased heat recovery (Crooijmans et al., 2016; Willems et al., 2017b), therefore making a geothermal system more profitable. As noted by Willems et al. (2020), current geothermal projects in the WNB demonstrate that the aquifer geology is still not fully understood. Increased knowledge on~~f~~ the regional architecture of the sedimentary formations~~rocks~~ hosting aquifers, the subsurface ~~seismic structural~~ geology, and the aquifer properties ~~such as stratigraphic architecture, thickness and heterogeneity~~, would help to de-risk the geothermal well planning in the area (Willems et al., 2020).

Presently, the main target for geothermal exploration in the WNB is the Jurassic Nieuwerkerk Formation (Willems et al., 2017c; Vondrak et al., 2018). This formation was interpreted as deposited in a fluvial-deltaic environment during the main rifting phase that shaped the basin, resulting in sharp lateral thickness and facies variations (van Wijhe, 1987; den Hartog Jager, 1996; Willems et al., 2020). Subsequent basin inversion, which started during the Late Cretaceous, caused uplift and deformation of~~within~~ the Nieuwerkerk Formation (e.g. van Wijhe, 1987; van Balen et al., 2000; de Jager, 2003; Deckers and

van der Voet, 2018). This tectonic history makes the reconstruction of the Jurassic tectono-sedimentary sequence, and therefore the thickness of its reservoir rocks more complex.

The quality of the recently reprocessed and released L3NAM2012AR ~~seismic~~ 3D depth migrated seismic cube allows for a detailed reconstruction of the main tectonic~~subsurface~~ structures. In contrast ~~Contrasting~~ to previous studies that mainly focussed on the NW-part of the onshore WNB (e.g. DeVault and Jeremiah, 2002; Willems et al., 2017c; Vondrak et al., 2018), now the SE-part of the onshore WNB could be integrated into the study area as well. The L3NAM2012AR 3D seismic cube was used to provide~~Accordingly, this study gives~~ a detailed interpretation~~overview~~ of the subsurface~~-seismic structural~~ geology, improving the knowledge of ~~and increases the knowledge of~~ the regional aquifer architecture, with a focus on the Nieuwerkerk Formation.

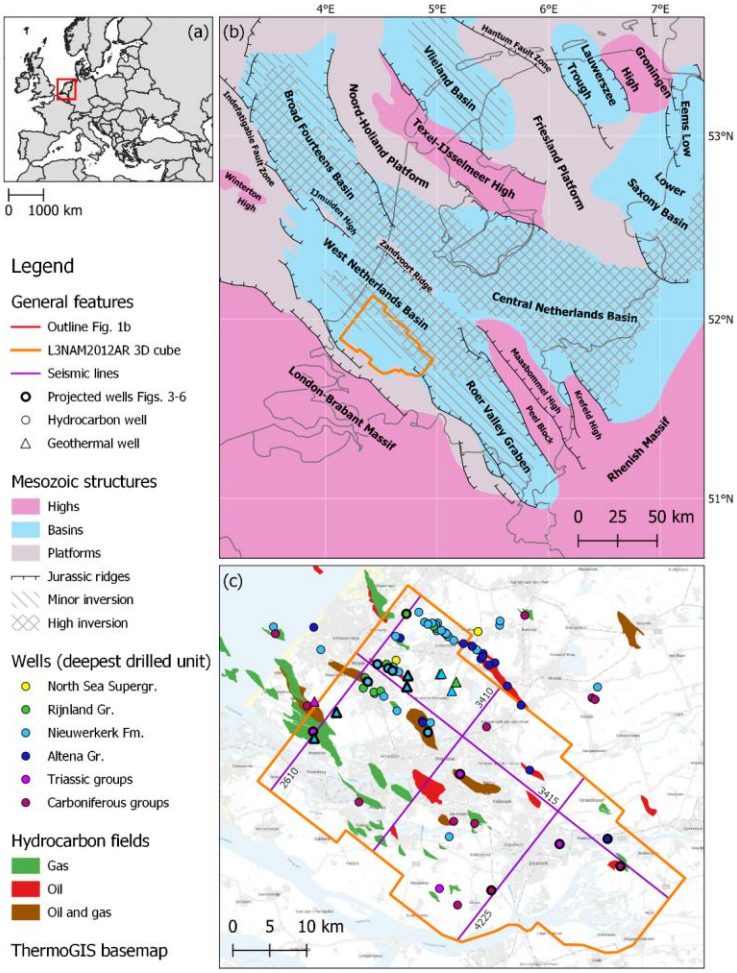

Figure 1: (a) Location of Figure 1b on the European continent. (b) Map of the Netherlands, showing the main structural elements during Jurassic times with the areas affected by the subsequent Late Cretaceous and Cenozoic inversion marked. The seismic 3D cube is displayed in orange. This map was produced by combining the maps from Wong et al. (2007) & Kombrink et al. (2011). (c) Map of the study area, highlighted in orange, showing all used wells with their colours delineating referring to the deepest encountered formation, the hydrocarbon fields and the seismic cross sections presented in figures 3, 4, 5 and 6.

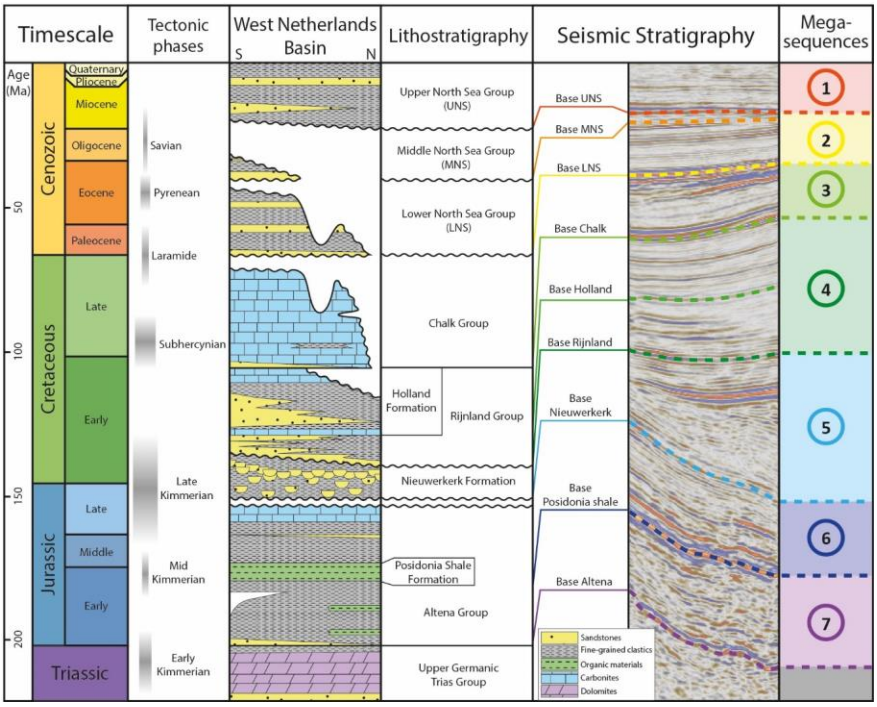

Figure 2: Lithostratigraphic chart, showing the timing of tectonic events, the simplified stratigraphy of the studied section of the West Netherlands Basin, ~~age of key horizons,~~ the interpret horizons and their age, and the typical seismic stratigraphy for the study area. Stratigraphic column adapted from van Adrichem Boogaert & Kouwe (1993) & Jeremiah et al. (2010) and the timing of tectonic events adjusted from Wong et al. (2007) with the results from this study.

2 Geological framework

The West Netherlands Basin (WNB) is a NW-SE elongated basin in the western sector of the onshore Netherlands (Fig. 1~~a~~). The WNB developed above a former Paleozoic basin, forming part of the Southern Permian Basin, and partly retraces its structural trend (e.g. Ziegler, 1992; van Balen et al., 2000; Michon et al., 2003; Worum et al., 2005). Break-up of Pangea marked~~s~~ the onset of E-W oriented extension in NW Europe at the beginning~~by the start~~ of the Mesozoic (e.g. Ziegler, 1992). Regionally, the Triassic is characterised by uplift due to the Early Triassic Hardegsen tectonic phase (Geluk et al., 1996) and the Late Triassic Early Kimmerian tectonic phase (Geluk and Röhling, 1997). An Early Jurassic faulting phase is recognized

in the area, causing differential subsidence in the basin's various subdomainsunits (van Balen et al., 2000), followed by Middle Jurassic uplift, referred to as the Mid Kimmerian tectonic phase (Herngreen et al., 2003).

Despite the tectonic phases mentioned above, Late Permian to Middle Jurassic times are generally considered to be part of the pre-rift stage within the WNB (e.g. den Hartog Jager, 1996; Racero-Baena and Drake, 1996; van Balen et al., 2000; Vondrak et al., 2018; Willems et al., 2020). The WNB, characterised by horst and graben structures, formed from theis considered to be Late Jurassic (Kimmeridgian) to Late Cretaceous (Barremian), therefore this period is marked as the syn-rift phase (van Wijhe, 1987; den Hartog Jager, 1996; de Jager, 1996; Racero-Baena and Drake, 1996; Vondrak et al., 2018). In particular, the WNB developed during several short discrete pulses, of short duration from which the strongest phasemain one, known as the Late Kimmerian tectonic phase, occurred during the Late Jurassic, recognized as the Late Kimmerian tectonic phase (van Wijhe, 1987; de Jager, 1996; Racero-Baena and Drake, 1996; van Balen et al., 2000). RThe rifting produced a main fault trend oriented NW-SE and caused resulted in the fragmentation of the WNB in several sub-basins, resultingwhere local differential subsidence resulted in large thickness variations within the Late Jurassic basin infill. After the endconclusion of the rifting phases by the Albian, the WNB underwententered a post-rift subsidence phase (van Wijhe, 1987), until basin inversion occurred, spanning from the Late Cretaceous to the Miocene (e.g. Ziegler, 1992; de Jager, 2003; Worum and Michon, 2005; Deckers and van der Voet, 2018; Kley, 2018).

The Late Permian to Cenozoic sedimentary succession of the WNB, described in detail byin van Adrichem Boogaert and Kouwe (1993) and TNO-GDN (2023), starts with the Late Permian Zechstein Group. The very few deep wells that have been drilled into the Zechstein Group have encountered carbonates and shales, but no evaporites. This group is overlain by the clastic Triassic Under-Germanian Group, which includes the Volpriehausen, Detfurth and Hardegsen formations. On top, the Middle to Late Triassic Upper-Germanian Group is made of mixed carbonates and (silici)clastics. Our seismic interpretation focused onstarts with the overlying Early to Middle Jurassic Altena Group (Fig. 2), which is primarily composed of shallow-marine clays, but also carbonates and sandstones. The Altena Group includes the Posidonia Shale Formation, which forms a key seismic reflector (Fig. 2). In the study area, the overlying Late Jurassic-Early Cretaceous Schieland Group includes only the Nieuwerkerk Formation, which is one of the main targets for geothermal exploration in the WNB (see above). It is characterised by lateral thickness variations associated with extensional faulting, and includes sandstones and shales that are both vertically stacked and laterally interfingered. TAbove is positioned the overlying Cretaceous Rijnland Group, which includes the Vlieland Subgroup and Holland Formation. The clastics of the Vlieland Subgroup were deposited in a transgressional setting that turned into a shallow to deep marine environment in which the carbonate and siliciclastic sediments of the Holland Formation were deposited. The Late Cretaceous carbonates of the Chalk Group were deposited in a shallow marine environment during the main inversion phase. The Cenozoic succession is known as the North Sea Supergroup,

composed of the clastics of the Lower, Middle and Upper North Sea Groups (e.g., van Adrichem Boogaert and Kouwe, 1993; Duin et al., 2006).

3 Data and methods

This study uses the L3NAM2012AR ~~seismic~~ 3D seismic depth cube and well data (Fig. 1c~~b~~), which recently became publicly available and can be downloaded from~~on~~ https://www.nlog.nl/datacenter/~~;~~. Additional technical details, including the reprocessing report and the acquisition, processing and interpretation work that was done before the reprocessing, can be found on the same website, using the provided steps described in the Supplementary Materials. ~~along with technical information (including data and procedure for depth conversion) about the survey.~~ The seismic coverage has a surface area of roughly 12~~3~~00 km^2, with 2678 diplines (2500-5178) and 1714 strikelines (2273-3987), penetrating to a depth of 6 km. The 3D cube was depth reprocessed and converted by Shell in 2011, using 59 wells for the depth conversion. We will use the depth converted version of this seismic cube, as the velocity cube ~~i~~is not publicly available (first of September 2023). Additional wells are available, from which we have used a total of 94 inside and 31 close to~~by~~ the study area, with a maximum depth of 4 km, and the deepest drilled formation being the Carboniferous Limburg Group (Fig. 1c). Specifically, for those wells, the gamma ray logs in combination with ~~The well database, together with~~ the available formation tops made it possible~~helped~~ to tie the wells to the seismic data. This allowed the calibration of the age of the main seismic horizons and sequences~~the seismic interpretation~~. Yet, some of the used wells date~~d back~~ from the start of hydrocarbon exploration in the basin in the 50's, and with the lithostratigraphic nomenclature changing over time, not all available formation tops are matching~~.~~~~,~~ This includes formation and group boundaries that are not used anymore. Therefore, ~~wherefore the~~ unmatching well tops were neglected.

We performed the seismic a~~A~~nalysis and interpretation ~~is done~~ using Petrel 2020.3 software, following the well-established workflow for interpretation of seismic datasets in extensional settings (e.g. O'Sullivan et al., 2022)~~.~~~~,~~ We interpreted the main faults and defined the seismic ~~which involves a reconstruction of the seismic~~ stratigraphy by integrating the well data in order to date the main ~~with the identification of different~~ seismic units~~facies~~, unconformities, and brightly marked reflective horizons. In detail, ~~9~~nine horizons were interpreted for the whole 3D cube (Fig. 2). Such a 3D interpretation has allowed us to identify the major faults of the basin and produce thickness maps of the pre-, syn-, and post-rift deposits, shedding light on the tectono-sedimentary evolution of the ~~single~~ sub-basins. ~~For the horizon interpretation, seismic-to-well tie was achieved by using the available well tops provided by TNO on nlog.nl. For each horizon, a grid of 25 diplines x 25 strikelines was made using a guided approach (guided autotracking + seeded 3D tools of Petrel). A continuous checking of the geological consistency of the interpretation was carried out during the interpretation, by considering the seismic facies of the mapped horizons and the occurrence of regional unconformities, as illustrated in Figure 2.~~

~~In detail, the bases of the Cenozoic Upper, Middle and Lower North Sea Groups, the base of the upper Cretaceous Chalk Group, the bases of the lower Cretaceous Holland Formation and Rijnland Group, the base of the upper Jurassic Nieuwerkerk Formation, the Posidonia Shale Formation and the base of the Altena Group were mapped (Fig. 2).~~ The nine~~ose~~ horizons were

selected either for their easily recognizable seismic facies or for their structural appearance (e.g. unconformities). For the horizon interpretation, seismic to well tie was achieved by using the available well tops provided by TNO on nlog.nl. In particular, the bases of the Cenozoic Upper, Middle and Lower North Sea Groups form angular unconformities, all easily recognized by their bright troughs that match the provided well tops very well. The clastic package of this Supergroup is defined by sub-horizontal, parallel reflectors. The base of the upper Cretaceous Chalk Group is represented by a bright peak that is easy to track, lying mainly conform upon the underlying strata, with some local unconformable contacts. The Chalk Group comprises sub-horizontal reflectors in its upper part, showing some local folds in its central and lower parts that are separated from the overlying reflectors by a local unconformity. The base of the lower Cretaceous Holland Formation, part of the Rijnland Group, is defined by a trough that lies conformably upon the underlying strata. The base of the Rijnland Group is defined by a dull peak that is not easy to track. Here, the well tops are needed to confine its location inside the sub-basins. The marine infill of the Rijnland Group forms parallel reflectors, affected by faults and folds. Overall, the reflectors of the Holland Formation show a brighter reflectance compared to the underlying unit of the Rijnland Group. The base of the upper Jurassic Nieuwerkerk Formation is defined by a trough that has an overall bright appearance, easy to track in the sub-basins using the provided well tops. Overall, the Nieuwerkerk Formation lies conformably upon the underlying package, yet some unconformable contacts are present. The package shows a range of seismic facies; going from bright parallel to chaotic reflectors. The bases of the Posidonia Shale Formation and Altena Group are easy recognizable by their bright troughs. They are defined by a combination of bright and dull parallel reflectors with locally some chaotic reflectors, all affected by faults and folds.

For each horizon, a grid of 25 diplines x 25 strikelines was made using a guided approach (guided autotracking + seeded 3D tools of Petrel). A continuous checking of the geological consistency of the interpretation was carried out during the interpretation, by considering the seismic facies of the mapped horizons and the occurrence of regional unconformities, as illustrated in Figure 2. The results section will describe three diplines and one strikeline that cover the study zone and are considered representative for all structures found in the seismic 3D cube (FFigs. 3-6). All four seismic sections were flattened for the base of the Rijnland Group. Despite all the limitations and biases of the flattening procedure, the flattened sections provide insights in the thickness variations of the Rijnland Group and underlying Nieuwerkerk Formation. Also, six thickness maps and a depth map will be discussed (Fig. 7). Thickness maps were made for the Middle and Lower North Sea Groups combined, the Chalk Group, the Rijnland Group, the Nieuwerkerk Formation, the upper half of the Altena Group (up to the base of the Posidonia Shale Formation) and the lower half of the Altena Group (megaquences 2-7 respectively, Fig. 2). The depth map was produced for the Upper North Sea Group (megasequence 1, Fig. 2). The thickness maps for each unit wasere produced in Petrel by computing the difference in elevation between the bounding horizonsbase of the overlying package and the base of the package itself. Although such a difference is not the actual thickness, given the horizons are characterised by very gentle dip (mostly less than 5°), it represents a reliable proxy. Exceptions are those areas of steeply dipping layers associated with tight folds. Also, the difference in elevation returns artefacts across faults, in which the top and bottom horizons

are located in the hanging wall and footwall, respectively. Those two exceptions are recognisable in maps as narrow ribbons of anomalous thickness values, mostly overlapping the major faults.

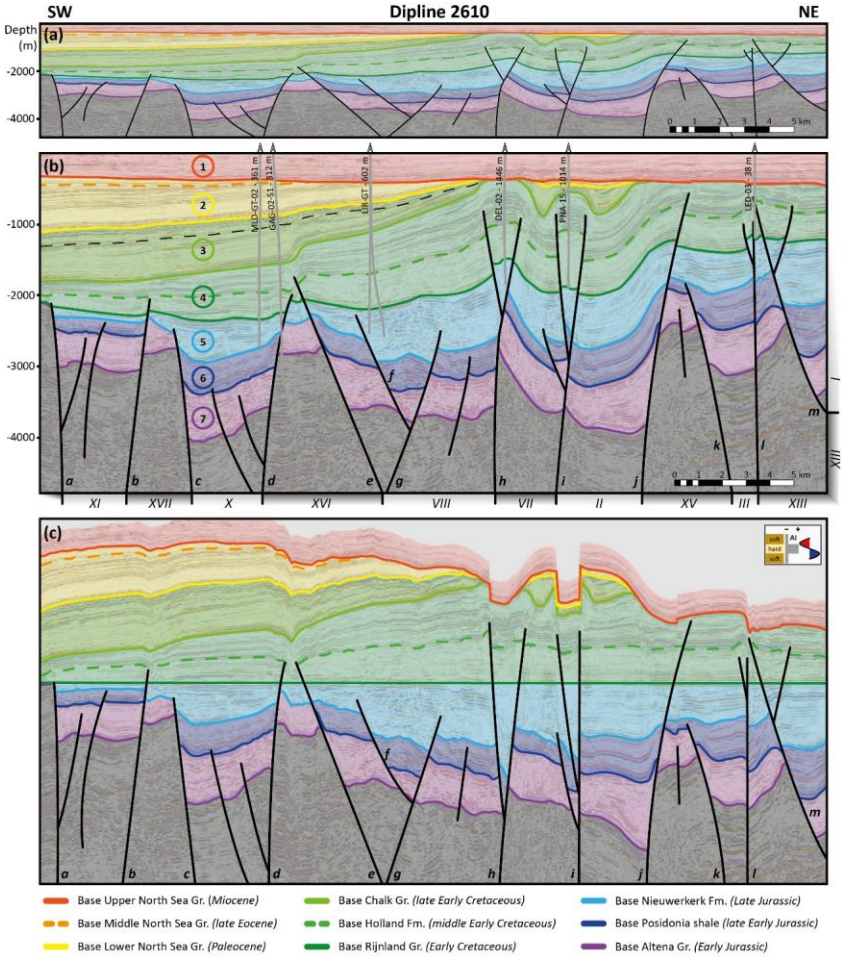

Figure 3: Dipline 2610 displayed with three different scales; (a): 1:1 scale, displayed with the interpreted horizons, megasequences and faults; (b): 1:3 scale, displayed with the interpreted horizons, megasequences and faults, together with projected wells and their distance to the seismic line, and the unconformity within megasequence 3 (marked by the black dotted line). Below the section, the sub-basins and highs are numbered as in Figure 7 ((XI): Voorne Graben, (XVII): Hoek van Holland High, (X): Maasland Graben, (XVI): De Lier High, (VIII): Westland Graben, (VII): Rijswijk Graben, (II): Voorburg Graben, (XV): Zoetermeer High, (III): Zoetermeer Graben, (XIII): Moerkapelle High, (I): Waddinxveen Graben); (c): the 1:3 scaled section flattened for the base of the Rijnland Group, displayed with the interpreted horizons, megasequences and faults.

4 Results

4.1 Seismic sections

Here we present three SW-NE sections oriented perpendicular to the main trend of faults affecting the WNB, and one section oriented NW-SE (Fig. 1cb). Up to the top of the Triassic, the stratigraphic succession can be divided into seven megasequences, here described from top to bottom. For each section, we present a 1:1 and 1:3 vertically exaggerated interpreted lines, along with a 1:3 vertically exaggerated one, flattened to the base of the Rijnland Group. The non-interpreted sections can be found in the Supplementary Materials.

4.1.1 Dipline 2610

Dipline 2610 (Fig. 3) is located on the NW edge of the study area (Fig. 1cb). The section is crosscutting the Pijnacker (PNA-15) and Rijswijk (DEL-02) abandoned oil fields, and the Gaag (GAG-02-S1) and the De Lier (LIR-GT wells) producing gas fields. The Leidschendam (LED-03) abandoned gas field and two producing open loop geothermal energy projects (MLD-GT-02 & LIR-GT wells) are nearby.

Megasequence 1 is positioned between the top of the seismic cross-section and the base of the Upper North Sea Group. The package is characterised by sub-horizontal reflectors and an evident erosional surface at the bottom, forming an angular unconformity and a toplap surface. Megasequence 2 underlies is found beneath this erosional surface, towards the SW. This megasequence is eroded in the NE part of the section and contains the Middle and Lower North Sea Groups. To the SW, the package is slightly tilted, dipping a few degrees towards the SW. An unconformable contact divides megasequences 2 and 3. In detail, tTowards the SW, reflectors of megasequence 2 and 3 are parallel to each other, whereas megasequence 2 erodes the top of megasequence 3 in the Westland Graben (structure VIII, Fig. 3b)., This leaves a local angular unconformable contact between megasequences 2 and 3an erosional unconformity is dividing them (the unconformity is also found in the well PNA-15, Fig. 3b). Megasequence 3 is composed of the Chalk Group, which is thins from 700 m to 0 mning towards the NE. Around well PNA-15, we observe two growth synclines capped by the unconformity that underlieswith the overlying megasequences 1 and 2. The upper part of this megasequence 3 is locally separateddivided from the central and lower ones by an unconformity (dashed black line, Fig. 3b). The apparent NE-ward thinning of this megasequence is mostly due to erosion, which is marked by the erosional surface that marksat the base of megasequence 1. The underlying megasequence 4 comprises the Rijnland Group. Opposeditely to megasequences 2 and 3, this package is thinning from 1000 m to 350 m towards the SW and it is affected by synclines and fault-cored anticlines, across whichwith no remarkable thickness changes are observed, as illustrated in the flattened section (Fig. 3c). Despite some local thickness anomalies (associated with the flattening procedure and the presence of faults) the flattened profile shows that megasequence 4 has a regional thinning towards the SW, which , which does is not considerably affected by change across the faults and folds. It is worth mentioning that observednone of the major faults affect the upper part of megasequence 4 and megasequences 5, 6 and 7seen in the section propagates across the upper portion of megasequence 4, with leaving the youngest three megasequences being un-faulted. Megasequence 5, which

corresponds to the Nieuwerkerk Formation, is characterised by abrupt thickness changes (with its thickness ranging between 100 m to 900 m) across the numerous faults affecting the megasequence. Below, megasequence 6, composed of the upper part of the Altena Group and based by the Posidonia Shale Formation, is characterised by parallel reflectors and thickness variations (its thickness ranges from 700 m to 0 m) related to erosion atop structural highs. Finally, megasequence 7, comprising the lower part of the Altena Group, displays both parallel reflectors and a few growth geometries at fault-bounded sub-basins.

The seismic line crosses 12 major faults. Some of them display normal offsets, while others show normal offset in the lowermost tracts and reverse displacement in the upper portions, which is a diagnostic feature of fault inversion (Williams, 1989). All major faults affect the megasequences 5 to 7, whereas only those showing evidence of positive inversion propagate into megasequence 4. As previously mentioned, megasequences 1 to 3 are un-faulted. In detail, faults labelled *a* to *d*, define horst and graben/half-graben structures. In the grabens/half-grabens ~~structures~~, megasequence 5 is characterised by ~~half-grabens~~growth geometries, whereas in the horst the thickness of megasequences 5 to 7 is strongly reduced (going from 550 m on the horst to 1400 m in the graben). None of these faults show remarkable evidence of inversion and the lowermost part of megasequence 4 seals all of them. Faults *e* and *h* bound a pop-up structure resulting from the inversion of these two former normal faults and the uplift of the pre-existing~~previous~~ sub-basin depocenter. Faults *f* and *g*, which show no evidence of inversion, were part of the array of extensional faults within this depocenter. In detail, the inversion of the SW boundary fault *e* caused fault-propagation-folding registered by "contractional" growth strata in megasequence 3. Inversion of the NE boundary fault *h* was accompanied by the development of an antithetic fault, forming a second-order pop-up structure that is affecting megasequence 4. To the NE, the SW-dipping fault *i* is ~~SW-dipping and~~ syn-sedimentary with respect to megasequence 5. Its inversion is accompanied by the development (or inversion) of two conjugate NE-dipping faults and resulted into a~~produces another~~ second-order pop-up structure, which controlled the deposition of~~whose development is recorded by growth geometries in~~ megasequence 3. Fault *j* displays evidence of positive inversion and, more importantly, bounds a half-graben (the Voorburg Graben, structure II, Fig. 3b) in which megasequence 7 displays ~~clear evidence of~~ growth-wedge geometries~~y~~. The NE-dipping fault *k* is also bounding ~~a semi-graben (~~the Zoetermeer Graben~~,~~ (structure III, Fig. 3b) in which ~~both~~ megasequences 5 and 7 ~~are characterised~~ show thickness variations; 400 m to 500 m for megasequence 5 and 500 m to 600 m for megasequence 7~~by thickness variations~~. Accordingly, the fault was~~has been~~ active during the deposition of megasequences 5 and 7. It is worth mentioning that it has not been reactivated during inversion. F~~Last, f~~ault *l* is NE-dipping and was~~has been~~ active during deposition of megasequence 5. This is evidenced by the flattened section, showing that the package of megasequence 5 is about 100 m thicker on the NE-side of the fault *l*, compared to the SW-side (Fig. 3c). It is slightly inverted as suggested by the gentle anticline deforming megasequence 4. Apart from the clear evidence of reverse offset on normal faults, folding of reflectors both in the hanging~~-~~wall and footwalls of some faults (e.g. in the footwall of fault *l* or in the hanging wall of faults *e* and *k*), reveals possible buttressing effect (i.e. folding and second order faulting o~~f~~n the hanging wall and footwall without slip reversal along the master fault).

heeft opmaak toegepast: Lettertype: Cursief

4.1.2 Dipline 3410

Dipline 3410 (Fig. 4) is located 16 km to the SE of dipline 2610 (Fig. 1c~~b~~). The section crosses the Rotterdam and Oud-Beijerland Noord producing oil fields and the Pernis and Hekelingen producing gas fields. Close-by are the IJsselmonde (IJS-64-S2) and Berkel (BRK-07) abandoned oil fields.

M~~Also here, m~~egasequence 1 shows sub-horizontal reflectors underlain by an~~based on an~~ extensive erosional surface. I~~Below, i~~n the SW part of the section, the underlying megasequence 2 shows gently tilted to parallel reflectors that are~~become~~ eroded towards the NE. A~~gain, a~~n unconformable contact separates megasequences 2 and 3, the latter show~~sing a~~ substantial thinning from 700 m to 0 m towards the NE ~~as well~~. Megasequence 3 forms~~displays~~ low-amplitude synclinal and anticlinal structures, well defined~~evident~~ at its base, capped by the unconformably overlying megasequence 2. Similarly to the seismic line shown in Figure 3, ~~also in this line~~ we observe a gently folded~~n~~ unconformity between the uppermost part ~~of the megasequence 3~~ and the central and lower parts of megasequence 3~~it~~ (black dashed line in Fig. 4b)~~., such an unconformity appears to be gently folded. The underlying m~~Megasequence 4 shows parallel reflectors thinning from 1000 m to 200 m towards the SW~~, as well evident in the flattened seismic profile~~ (F~~F~~igs. 4a and c), which are disrupted by faults. In the NE part of the section, the megasequence is partly eroded and directly toplapping onto megasequence 1. M~~None of the m~~ajor faults affect the upper lower part of megasequence 4, and megasequences 5, 6 and 7 ~~propagate across the top part of megasequence 4~~, whi~~lech leaves~~ the youngest three megasequences are un-faulted. M~~Below, m~~egasequence 5 is affected by ~~a number of~~ faults *d*, *n*, *h*, *o*, *i* and *k*, ~~and~~ displaying~~s~~ abrupt thickness changes ranging from 400 m to 1300 m. These thickness changes are even more clearly visible on the flattened section ~~(despite all the limitations and biases of the flattening procedure)~~., ~~where~~ t~~T~~he package shows at least four distinct asymmetric fault-bounded half-grabens. ~~Also here, t~~The underlying megasequence 6 is characterised by parallel reflectors and, contrasting to section 2610, megasequence 6 does not show significant thickness changes, having an average thickness of 450 m. The lowermost megasequence 7 displays both parallel layers, slight thickness changes (ranging from 500 m to 850 m) and a fault-bounded half-graben in the Zoetermeer Graben (structure III, Fig. 4b)~~at the NE part of the section~~.

Seven major faults are recognized in this seismic section, both normal and partially (in the lowermost tracts) inverted. The faults affect M~~m~~egasequences 5 to 7 ~~are affected by all the faults~~, whereas only the faults showing positive inversion cut through~~are propagating into~~ megasequence 4~~., leaving megasequences 1 to 3 un-faulted. Part of the~~ Some faults (*c*, *d*, *h*, *i* and *k*) recognized in ~~from~~ dipline 2610 are also mapped ~~extend~~ in this section. In detail, faults *c* and *d* bound a structural high (the De Lier High, structure XVI, Fig. 4b)~~, describing with~~ small horst and graben structures. M~~Here, m~~egasequence 5 is absent in this region and the horst and graben, and the bounding ~~both structures and~~ faults are sealed~~capped~~ by the uppermost part of megasequence 4. Fault *c* and the smaller faults within the bound structure show notable evidence of inversion, as evidenced by the antithetic fault connected to fault *c*. However, contrasting to section 2610, where fault *d* does not display evidence of~~clues of~~ inversion, the ~~here~~ inversion of this fault in this section~~the NE boundary of fault *d*~~ resulted in the development of antithetic fault *n*. Together, the faults formed a set of small pop-up structures ~~and a fault propagation fold atop fault *n*~~, recorded

heeft opmaak toegepast: Lettertype: Cursief
heeft opmaak toegepast: Lettertype: Cursief
heeft opmaak toegepast: Lettertype: Cursief
heeft opmaak toegepast: Lettertype: Cursief
heeft opmaak toegepast: Lettertype: Cursief
heeft opmaak toegepast: Lettertype: Cursief
heeft opmaak toegepast: Lettertype: Cursief

byregistered in a fault-propagation fold atop fault *n* in megasequence 4. The SW dippingF faults *h* and *i* show a similar geometry, being SW-dipping controlled by the deposition ofand syn-sedimentary with respect to megasequence 5. Inversion of both faults waiis accompanied by the development of fault-propagation folds in megasequence 4. BIt ©s interesting to mention that both faults formed second-order pop-up structures in section 2610. FIn between faults *h*, and *i* , and fault *o* is recognized and together, these three faults bound two elegant semi-grabens (the Rijswijk and Pijnacker grabens, (structures VII and IV, Fig. 4b). In these structures, in which megasequence 5 shows clear growth geometries. Inversion of fault *o* caused the development of an antithetic fault, forming a second-order pop-up structure. TBoth the development of the fault-propagation folds and the second-order pop-up structure as result of the inversion of faults *d*, *h*, *o* and *i* recorded by growth geometries in megasequence 3 recorded the development of the fault-propagation folds and the second-order pop-up structure as result of the inversion of faults *d*, *h*, *o* and *i*. FLast, also here, fault *k* bounds is not inverted, but more importantly, it is bounding a semi-graben (the Zoetermeer Graben, (structure III, Fig. 4b) in which both megasequences 5 and 7 showare characterised by thickness variations ranging from 600 m to 800 m for megasequence 5 and from 800 m to 400 m for megasequence 7. Like in section 2610, evidence for fault inversion is clear with folding of reflectors (e.g. in the hanging wall of fault *d* and footwall of fault *i*) suggestsrevealing a buttressing effect upon inversion.

heeft opmaak toegepast: Lettertype: Cursief

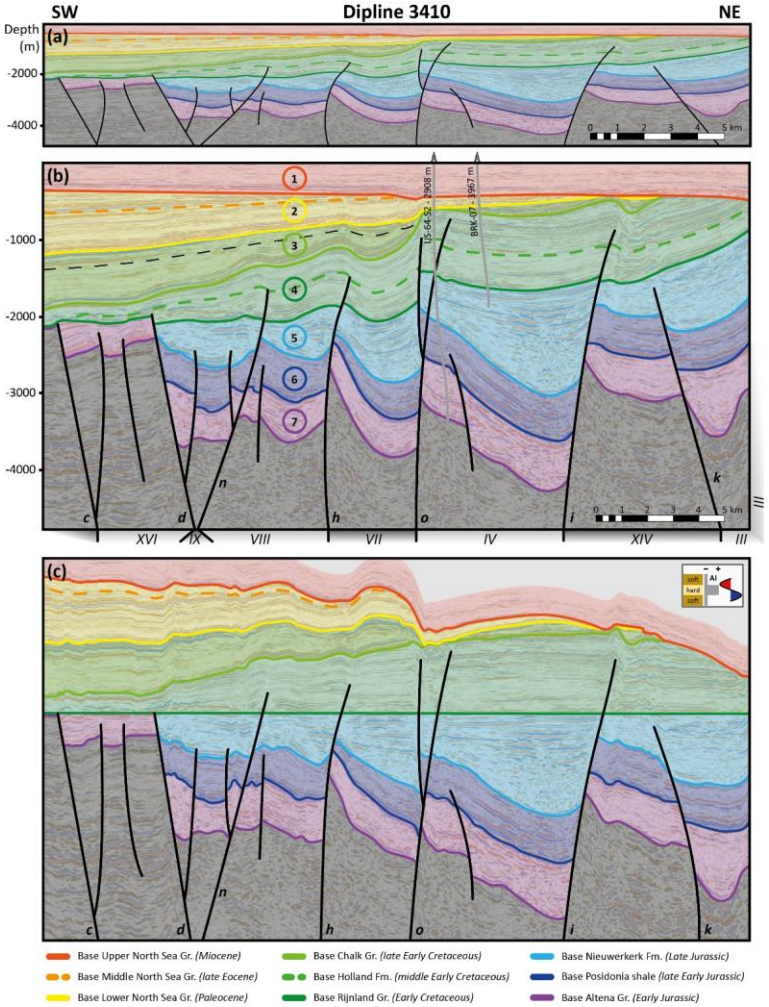

Figure 4: Dipline 3410 displayed with three different scales; (a): 1:1 scale, displayed with the interpreted horizons, megasequences and faults; (b): 1:3 scale, displayed with the interpreted horizons, megasequences and faults, together with projected wells and their distance to the seismic line, and the unconformity within megasequence 3 (marked by the black dotted line). Below the section, the sub-basins and highs are numbered as in Figure 7 ((XVI): De Lier High, (IX): Spijkenisse Graben, (VIII): Westland Graben, (VII): Rijswijk Graben, (IV): Pijnacker Graben, (XIV): Lansingerland High, (III): Zoetermeer Graben); (c): the 1:3 scaled section flattened for the base of the Rijnland Group, displayed with the interpreted horizons, megasequences and faults.

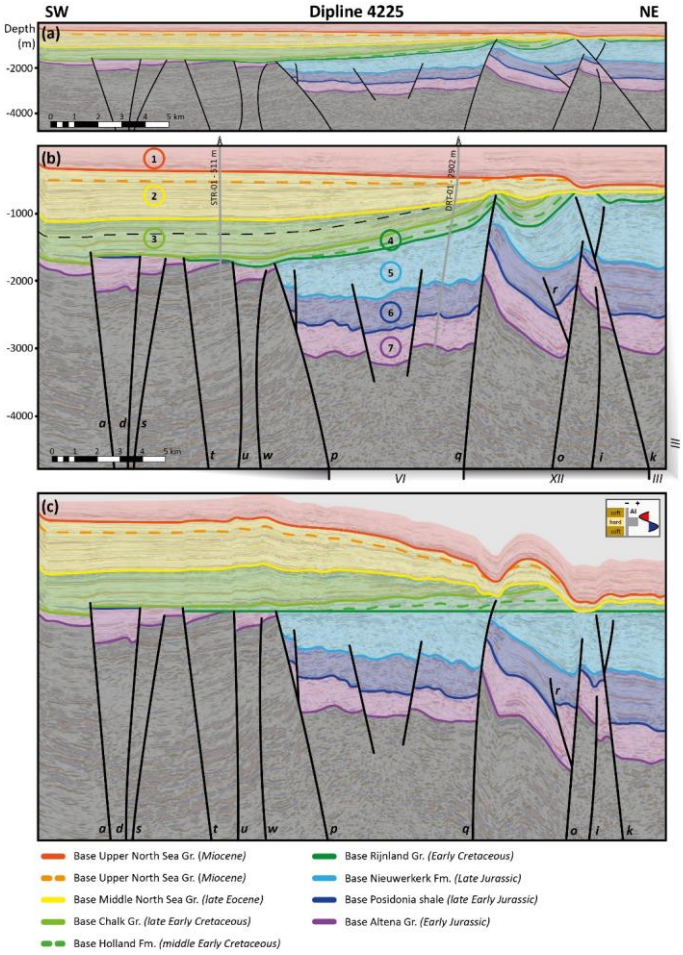

Figure 5: Dipline 4225 displayed with three different scales; (a): 1:1 scale, displayed with the interpreted horizons, megasequences and faults; (b): 1:3 scale, displayed with the interpreted horizons, megasequences and faults, together with projected wells and their distance to the seismic line, and the unconformity within megasequence 3 (marked by the black dotted line). Below the section, the sub-basins and highs are numbered as in Figure 7 ((VI): Dordrecht Graben, (XII): Ridderkerk Graben, (III): Zoetermeer Graben); (c): the 1:3 scaled section flattened for the base of the Rijnland Group, displayed with the interpreted horizons, megasequences and faults.

4.1.3 Dipline 4225

Dipline 4225 (Fig. 5) is located 16 km SE of dipline 3410 ~~(Fig. 1b)~~ and it does not crosscut any wells of an hydrocarbon field or geothermal energy projects (Fig. 1c). From the projected wells (Fig. 5b), STR-01 resulted in oil and gas shows, while well DRT-01 was dry.

~~In this line, m~~Megasequence 1 shows subhorizontal reflectors, floored by a major erosional surface. Below, megasequence 2 shows gently dipping reflectors, that are truncated~~becoming eroded on top~~ by the basal unconformity of megasequence 1 towards the NE. Towards the SW, the underlying megasequence 3 shows parallel reflectors, which are also parallel to those of ~~parallel to~~ megasequence 2 ~~towards the SW~~, while ~~towards the NE,~~ above the Dordrecht ~~Graben~~ and Ridderkerk ~~G~~grabens (structures VI and XII, Fig. 5b) towards the NE, an unconformity ~~is separating~~separates these two megasequences. The intra-sequence unconformity that separates the uppermost and lowermost parts of megasequence 3 ~~from the lower part~~, which is also observed in diplines 2610 and 3410, is observed here as well (black dashed line in Fig. 5b). In the SW, megasequence 3 is affected by faults. ~~The underlying m~~Megasequence 4 is thin~~sning~~ from to 200 m to 0 m towards the SW~~,~~. ~~being affected by a~~A syncline and fault-cored anticlines deformed megasequence 4 towards the NE~~.~~, leading to erosion and the unconformable deposition of megasequence 2 on top. ~~Towards the NE, megasequence 4 gets eroded by both megasequence 2 and 3. Except for fault *a*, none of the faults propagates across the top part of megasequence 4. Below, m~~ Faults *a* and *g* crosscut the upper part of megasequence 4. Megasequence 5 is only present towards the NE portion of the section. Like in the previous diplines, megasequence 5 is affected by a number of faults (faults *p*, *q*, *o*, *i* and *k*) and shows abrupt thickness changes ranging from 1000 m to 0 m, even better visible on the flattened section (Fig. 5c). In the Ridderkerk Graben (structure XII, Fig. 5b), megasequence 5 forms a fault-bounded half-graben. The underlying megasequence 6 is characterized by parallel reflectors with an average thickness of 500 m, only showing a ~~thickness~~ change~~s~~ in thickness, ranging from 100 m to 750 m, in the NE part of the section in the Ridderkerk and Zoetermeer ~~G~~grabens (structures XII and III, Fig. 5b), related to erosion atop former structural highs. ~~Lastly, m~~Megasequence 7 is characterized by both parallel layers and slight thickness changes, well evident in the Ridderkerk and Zoetermeer grabens, where the thickness ranges from 300 m to 800 m.

Twelve major faults are recognized in this seismic section~~, from which eight will be described,~~ comprising both normal and partially (in the lowermost tracts) inverted faults. Megasequence~~s 5 and~~~~s 5 to~~ 7 are ~~are~~ affected by all displayed ~~all the faults~~faults, from which faults *a*, *p*, *q*, *o* and *k* ~~whereas only the faults~~ show~~ing~~ evidence of positive inversion. Fault *g* ~~-~~also affect~~s~~ megasequence~~s~~ 3, whereas faults *p* and *q* affect megasequence 4. Megasequence 3, is affected by an inverted fault (fault *a*), which is not occurring in ~~Contrasting to~~ diplines 2610 and 3410~~, megasequence 3 is affected by one inverted fault, fault *a*~~. M~~Above, m~~egasequences 2 and 1 are not affected by faults. F~~Part of the f~~aults ~~(~~*a*, *d*, *i*~~,~~ and *k*~~)~~, interpreted in ~~from~~ dipline 2610 and ~~part of the~~ faults ~~(~~*d*, *i*, *k*~~,~~ and *o*~~) from~~ traced in dipline 3410 ~~extend~~are also recognized in this section. The SW-side of fault *p* ~~represents~~marks the edge of the WNB~~, containing the four major faults that are not numbered,~~ with faults *a*, *d*, *s*, *t*, *u* and *w* forming horst ~~-~~and ~~-~~graben structures ~~(between faults *p* and *a*)~~. The infill of the horst and graben structures includes~~Here, only~~ megasequence 7 and a thin layer of 50 m of megasequence 6, which ~~is present and the structures~~ are capped by either

heeft opmaak toegepast: Lettertype: Cursief

heeft opmaak toegepast: Lettertype: Cursief

heeft opmaak toegepast: Lettertype: Cursief

heeft opmaak toegepast: Lettertype: Cursief

heeft opmaak toegepast: Lettertype: Cursief

heeft opmaak toegepast: Lettertype: Cursief

megasequence 3 or 4. Faults *a* and *d* ~~from the previous~~identified in sections 2610 and 3410 are also identified in seismic line 4225. ~~extent into this domain, from which f~~Fault *a* shows evidence of~~a~~ positive inversion~~,~~ (i.e., ~~resulting in~~ a small offset in megasequence 3~~)~~. This ~~is contrasting to~~contrasts with observations performed in section 2610, where fault *a* doesn't show inversion and is capped by megasequence 4. Faults *p* and *q* bound ~~a graben (~~the Dordrecht Ggraben~~,~~ (structure VI, Fig. 5b) that shows some internal normal faulting. ~~Both f~~Faults *p* and *q* show positive inversion ~~features~~ in their uppermost~~top~~ segments, evidenced by an antithetic fault in the upper part of fault *p* and the development of a fault-cored anticline in megasequence 4 atop fault *q*. Towards the NE, faults *q* and *k* bound ~~a half-graben (~~the Ridderkerk Graben~~,~~ (structure XII, Fig. 5b). ~~Below this semi-graben,~~Faults *o* and *k* bound a former structural high underlying this graben.~~can be found, bound by faults *o* and *k*. Similar to~~ As observed in section 3410, the inversion of fault *o* resulted in the development of an antithetic fault, here called fault *r*, which affects~~but here only~~ megasequences 6 and 7 in seismic line 4225.~~are affected by this antithetic fault.~~ Inside the former structural high, fault *i* is normally ~~faulting~~displacing megasequence 7. This ~~is contrasting to the previous sections,~~contrasts with observations in seismic lines 2610 and 3410, where fault *i* ~~is expressed as a major fault with~~shows positive inversion in the upper segment. Towards the NE, like in section 3410, fault *k* bounds the Zoetermeer Graben (structure III, Fig. 5b). ~~Contrasting to~~In contrast with observations performed in ~~the previous sections~~seismic lines 2610 and 3410, where fault *k* does not show evidence of inversion, ~~here~~ an antithetic fault formed in the upper segment as the result of reverse offset in seismic line 4225.

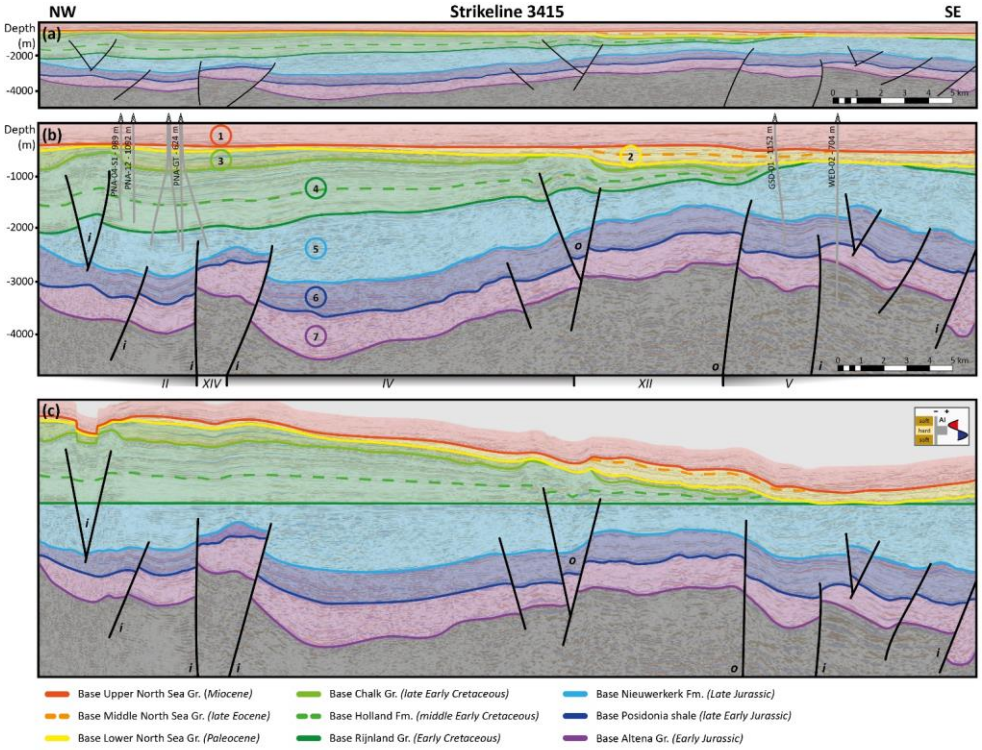

Figure 6: Strikeline 3415 displayed with three different scales; (a): 1:1 scale, displayed with the interpreted horizons, megasequences and faults; (b): 1:3 scale, displayed with the interpreted horizons, megasequences, faults and projected wells with their distance to the seismic line. The strikeline intersects fault i several times, wherefore the fault can be recognized multiple times. Below the section, the sub-basins and highs are numbered as in Figure 7 ((II): Voorburg Graben, (XIV): Lansingerland High, (IV): Pijnacker Graben, (XII): Ridderkerk Graben, (V): Biesbosch Graben); (c): the 1:3 scaled section flattened for the base of the Rijnland Group, displayed with the interpreted horizons, megasequences and faults.

4.1.4 Strikeline 3415

Strikeline 3415 (Fig. 6) runs perpendicular to the previously described lines, and crossinges the NE part of the study area (see Fig. 1b), the Werkendam abandoned oil field (WED-02) and the undeveloped Werkendam-Diep gas field (Fig. 1c). ClosebyNearby is the dry GSD-01 well, the Pijnacker (PNA-04-S1 & PNA-12) abandoned oil field and athe producing geothermal energy project (PNA-GT wells).

Megasequence 1 is characterised by subhorizontal reflectors and is ~~bottomed~~underlain by an erosional surface. Megasequence 2 is characterised by thickness variations ranging from 50 m to 350 m, associated with uplift and erosion.~~,~~ ~~whereas~~ Reflectors within megasequence 3 lap onto the limbs of anticlines cored by ~~displays growth geometries with respect to~~ faults *i* and *o*. Megasequence 2 toplaps megasequence 3, ~~the latter disappearing~~which wedges out from 400 m to 0 m towards the SE. The base of megasequence 2 represents and erosional surface that truncates ~~open~~open anticlines and synclines, ~~with evident~~showing erosion of megasequences 3, 4 and 5 at the hinges. Megasequence 4 includes parallel reflectors, has an average thickness of 1100 m in the Voorburg and Pijnacker grabens and Lansingerland High (structures II, IV and XIV), and ~~shows thinning~~thins to 0 m along Ridderkerk and Biesbosch grabens (structures XII and V) towards the SE ~~with parallel reflectors and no distinct thickness variations across short distances~~. Below, megasequence 5 is characterised by thickness variations ranging from 500 m to 1300 m across short distances. No clear boundary faults can be identified in this line for the growth-structures ~~hosted~~observed in megasequence 4, ~~evidencing~~corroborating the idea that the major faults are oriented at low angle to this seismic section. Also, the ~~within the package of~~reflectors within megasequence 5 show ~~, di~~differen~~t~~ti~~ng~~ appearances ~~of reflectors are observed~~; both parallel and chaotic reflectors with mixed bright and dull appearances are observed, pointing towards variations in~~of~~ seismic facies. ~~Underlying m~~Megasequence 6 does not show remarkable thickness variations, having an average thickness of 550 m. ~~whereas~~ The lowermost megasequence 7 shows some slight changes in thickness ranging from 400 m to 900 m.

As section 3415 crosscuts~~is oriented at a low angle to~~ the main faults at a low angle, ~~less intense~~relatively mildly deformation is ~~on and thickness variations are~~ observed. Fault *i* is ~~oriented~~ parallel to section 3415 and, ~~as it extends throughout the whole 3D cube, this fault crosses the section~~it can be interpreted several times along the section, suggesting that it extends throughout the whole 3D cube and ~~. The fault~~ bends along the section when going to the SE. Minor folding is observed in megasequence 4 ~~atop these sections~~along seismic section 3415 related to ~~of~~ fault *i*, but no distinct inversion structures are ~~present~~recognized. ~~The steep attitude of fault *i* suggests the occurrence of oblique segments along the trace of this fault.~~ Last, in the middle of the section, fault *o* bounds the Ridderkerk Graben (structure XII, Fig. 6b), and show~~s~~ing a related second-order pop-up structure on the NW-boundary of this horst, which is the same pop-up structure as observed along fault *o* in ~~related to fault *o* (~~section 3410~~) on the NW-boundary of this horst.~~. Except for the second-order pop-up structures related to faults *i* and *o* that are capped by megasequence 3, all ~~All faults, except the horst structures related to faults *I* and *o*,~~ faults are seale~~d~~d~~capped~~ by megasequence 4~~. , whereas the faults of the horst structures are capped by the top part of the latter.~~

heeft opmaak toegepast: Lettertype: Cursief

heeft opmaak toegepast: Lettertype: Cursief

heeft opmaak toegepast: Lettertype: Cursief

4.2 Thickness maps

~~Here, we present the thickness maps of megasequences 2 to 7 (Fig. 7b-g) and the depth map of the base of megasequence 1 (Fig. 7a).~~ Megasequence 1 represents the youngest unit and is bounded upwards by the seafloor, therefore the depth map of its base is representative of its thickness (Fig. 7a). Figures 7b to g display the thickness maps of megasequences 2 to 7. Overall, megasequence 1 shows a constant thickness of around 400 m. Towards the E, an abrupt increase in depth is observed, giving megasequence 1 thicknesses up to 650 m. This is related with th~~e~~e only fault crosscutting this megasequence, which is an

extension of fault ~~*k*~~ *k* (dipline 4225, Fig. 5b). Megasequence 2 ~~shows a general thinning~~thins from 800 m in the SW to 0 m towards the NE (Fig. 7b), due to the uplift and erosion that led to the development of the overlying erosional surface, as observed in all seismic lines (Figs. 3-6). ~~which is related to the overlying erosional surface, but we~~Within megasequence 2, we also observe the occurrence of narrow NNW-SSE and NW-SE elongated areas ~~with an increased thickness~~showing an increase in sediment thickness from 200 m to 500 m. As seen in all three~~the~~ seismic ~~cross sections~~diplines (F~~F~~igs. 3~~-5 and 4~~), megasequence 3 was deposited during faults' inversion, evidenced by thickness variations of up to 800 m that correspond to present folds (Fig. 7c).~~.~~

~~This latter packag~~The~~e displays an~~ overall NE-ward thinning from up to 800 m to 0 m is ~~,~~ related to erosion and due to basin inversion. The erosional surface at the base of megasequence 1 that is observed on all seismic sections (Figs. 3-6), led to the formation of ~~the overlying erosional surface that is present at the base of megasequence 1, with~~ both NNW-SSE and (mostly) NW-SE elongated areas where the thickness is reduced to 0 m ~~of increased/reduced thickness~~for both megasequences 2 and 3. ~~Contrasting to~~In contrast with thickness variations of megasequence 3, megasequence 4 displays an overall thinning from 1500 m to 0 m towards the S, with no localised areas of ~~increased~~maximum or ~~/~~minimum~~decreased~~ thicknesses (Fig. 7d). Megasequence 5 (the main geothermal target interval) is characterised by an overall thickness increase from 0 m to 1200 m towards the NE (Fig. 7e). NW-SE and NNW-SSE oriented faults bound ~~A~~areas of increased~~/~~ and reduced thicknesses that are mostly lozenge-shaped ~~with boundary faults being NW-SE and NNW-SSE oriented~~. Towards the S, the thickness of megasequence 5 is ~~almost~~ 0 m or close to 0 m, ~~absent~~ due to erosion and/or non-deposition. Sub-basins filled by megasequence 5 are asymmetric, as evidenced by the ~~sudden~~abrupt thickness changes ranging from 400 m to 1400 m that are observed towards the NE. This contrasts with the ~~compared to a~~ more ~~gentle~~progressive thickness decrease towards the SW, where the thickness decreases more gently from roughly 600 m to 0 m. Such an observation is suggestive of a first order architecture composed of half-graben~~s structures~~ bounded by SW-dipping master faults.

The interpretation of the thickness maps of megasequences 6 and 7 is ~~less straightforward~~more complex, as these megasequences experienced multiple tectonic events that caused faulting, folding and erosion. These thickness maps show the effects of erosion during the deposition of megasequence 5, e.g., in the horst structure between faults *b* and *c* in section 2610 (Fig. 3). This effect is seen in the map as NNW-SSE oriented ribbons of reduced thickness (roughly up to 1000 m difference in thickness compared to the surrounding topography), resembling horst structures. If we

heeft opmaak toegepast: Lettertype: Cursief

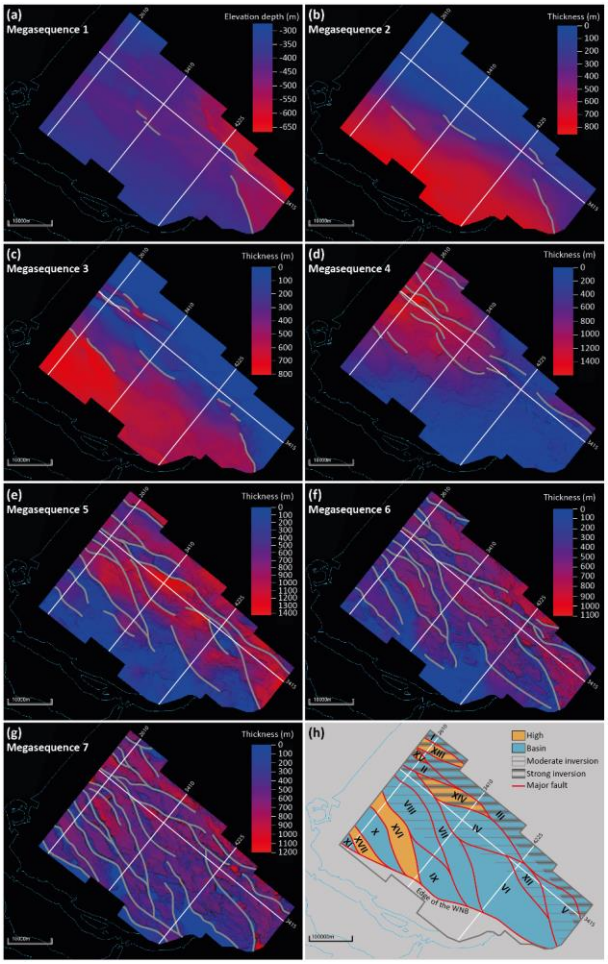

Figure 7: (a): Depth map of megasequence 1, with present faults displayed in grey; (b-g): thickness maps of megasequences 2–7 with present faults displayed in grey; (h): Simplified map showing the structural elements formed as consequence of the first and second rifting episodes, together with a qualitative estimation of the degree of inversion. The seismic section displayed in figures 3-6 are displayed, together with the different highs and basins, which are numbered and named; (I): Waddinxveen Graben, (II): Voorburg Graben, (III): Zoetermeer Graben, (IV): Pijnacker Graben, (V): Biesbosch Graben, (VI): Dordrecht Graben, (VII): Rijswijk Graben, (VIII): Westland Graben, (IX): Spijkenisse Graben, (X): Maasland Graben, (XI): Voorne Graben, (XII): Ridderkerk Graben, (XIII): Moerkapelle High, (XIV): Lansingerland High, (XV): Zoetermeer High, (XVI): De Lier High, (XVII): Hoek van Holland High.

remove~~Remove~~ the effect of those ribbons from the thickness maps of megasequences 6 and 7, and we rely on the occurrence of growth geometries (such as the growth wedge ~~seen~~observed in megasequence 7 in the Voorburg Graben, structure II, close to fault *j*, Fig. 3b), we can make some observations. Megasequence 6 displays thickness variations, ranging between 0 m and 1100 m (Fig. 7f). None of the thickener areas (between 600 m and 1100 m) show growth wedge geometries, suggesting that thickness variations relate to later erosion rather than to syn-sedimentary creation of accommodation space. ~~observe that the thickness distribution of m~~Megasequence 7 ~~displays~~describes NW-SE elongated graben~~s~~/semigraben~~s~~ where thicknesses can quickly change from 400 m up to 1200 m (Fig. 7g)~~.~~, The infill consists of asymmetrically wedge-shaped~~filled by~~ growth strata ~~wedging away from the master faults, and~~, which are separated by horst structures. The Lansingerland High is ~~A~~an outstanding example ~~occurs~~ in the northern corner of the map. This structure is~~, where a~~ a 20 km long NW-SE elongated horst (~~the Lansingerland High,~~ structure XIV, Fig. 7h) bounded by two depocenters ~~is observed~~ where the thickness changes from 400 m on the horst to 1000 m in the depocenters.~~.~~ ~~Megasequence 6 displays similar thickness variations, but none of the thickener areas show growth wedge geometries, suggesting that thickness variations relate to later erosion rather than to syn-sedimentary creation of accommodation space.~~

5 Discussion

5.1 Tectonic evolution

The interpretation of the L3NAM2012AR seismic 3D cube has allowed us to ~~subdivide the investigated sedimentary succession into~~define seven megasequences, ~~corresponding to units~~including sediments~~.~~ spanning in age from Jurassic to Present times. Megasequences are delimited either by ~~the occurrence of u~~unconformities (base of megasequences 1, 2, 4 and 5), or by the transition from unconformity~~growth geometries~~ (e.g. growth geometries, stratigraphic fanning/expansion-tapering, convergent reflectors) to correlative conformity (e.g. parallel geometries). ~~It is noted that i~~Intra-formational unconformities are ~~present~~also observed. However, in the framework of a reconstruction of the subsurface ~~sub-seismic structural reconstruction~~, only the main seismo-stratigraphic~~al~~ units are ~~taken into account~~defined. Based on our observations, the evolution of the studied portion of the WNB from the Jurassic onward can be assessed.

The first observed tectonic period can be dated to the Early Jurassic, which is the biostratigraphic age of the sedimentary rocks of megasequence 7. NW-SE elongated regions of decreased and increased ~~thickness~~thickness variations of up to 800 me~~s~~. (Fig. 7g) are interpreted as related to Early to Middle Jurassic fault-bounded horst and graben structures, respectively. Growth geometries within this megasequence are observed, like the half-graben in the Voorburg Graben (structure II, associated with fault *j*, Fig. 3b). Coherently, megasequence 7 is interpreted as a syn-rift sequence, with the thickness of syn-rift infill increasing with roughly 600 m towards the NE (Fig. 7g). Regionally, this rifting stage is synchronous with the final stage of the first rifting event that has shaped the North Sea Rift system (e.g. Fossen et al., 2021). This rifting event seems to coincide with the regionally recognized Early Kimmerian tectonics (Fig. 2) (Geluk and Röhling, 1997; Duin et al., 2006)~~.~~ The overlying megasequence 6 displays areas of slight thickness variations of up to 400 m (Fig. 7f). Erosion and non-deposition cause these

variations, such as on the former structural highs, like the Hoek van Holland, De Lier and Zoetermeer highs (structures XVII, XVI and XV, Fig. 3b)., ~~but n~~ No growth geometries are observed within megasequence 6~~occur in it~~, therefore, it is to be considered post-rift. Overall, both megasequence 6 and 7 display a slight NE-ward thickening (Figs. 7f and g), with the thickening direction being perpendicular to the direction of the main normal faults that were active during the Early Jurassic rifting stage. According to the widely recognised features in rift systems (e.g. Franke, 2013; Peron-Pinvidic et al., 2019), we interpret the creation of accommodation space synchronously with deposition of megasequence 7 and the overlying megasequence 6 as the post-rift passive infill ~~of the accommodation space created synchronously with the deposition of megasequence 7~~. Since the timing of deposition of megasequence 6 corresponds to the inception of the thermal North Sea Rift Dome underneath the central North Sea (van Wijhe, 1987; Ziegler, 1992), an alternative hypothesis could be that thinning of megasequence 6 is somehow related with this lithospheric-scale bulging process. Given the centre of the dome was located far N (between NW Scotland and SE Norway) (Ziegler, 1992; Wong et al., 2007), N-ward thinning of megasequence 6 should be observed, which is not the case. Yet, it should be noted that later structural evolution could have overprinted subtle effects related to the North Sea Rift Dome. Still, the absence of N-ward thinning makes us discard the hypothesis of doming causing large impact on the depositional pattern of megasequence 6.

Deposition of the overlying megasequence 5 started in the Late Jurassic, during a second pulse of extensional faulting. The observed local unconformities within megasequence 5 suggest that faulting happened in several pulses. This stage is coeval with the second phase of rifting observed in the North Sea, further to the N (e.g. Færseth, 1996), which induced an enhancement crustal extension, known as the Late Kimmerian tectonics (van Wijhe, 1987; Ziegler, 1992; de Jager, 1996; Racero-Baena and Drake, 1996; van Balen et al., 2000). In the WNB, this extensional phase is simultaneous with igneous activity (Sissingh, 2004), a characteristic of continental rifting (e.g. Franke, 2013; Gouiza and Paton, 2019). We observe that the upper portion of megasequence 5 postdates all the normal faults (excluding those showing evidence of reverse reactivation). Several syn-depositional wedges (most of them being half-grabens) are observed in this megasequence, such as those associated with faults *h*, *o* and *i* ~~in~~ (Fig.~~ure~~ 4). The various sub-basins active during this second extensional pulse are lozenge-shaped, ~~and they are~~ bounded by NW-SE and NNW-SSE striking faults (Fig. 7e)., ~~.~~ The Westland, Pijnacker, Dordrecht and Biesbosch grabens are good examples of this (structures VIII, IV, VI and V, Fig. 7h). T~~t~~heir ‘~~“~~zigzag’~~”~~ arrangement of faults are~~being~~ a typical feature when pre-existing faults occur (e.g., Henstra et al., 2019). ~~.~~ Many horst and graben~~s structures~~ active during this second rifting phase retrace structures developed during the first rifting stage, such as the ones seen in the NW part of the study area (e.g. the Westland and Pijnacker ~~G~~grabens, structures VIII and IV, Fig. 7h). The observation that during the first rifting stage the structures were NW-SE oriented, allowed us to infer that those NW-SE striking structures were reactivated during the second rifting phase. Accordingly, we deduce that the NNW-SSE striking normal faults formed during the second rifting phase. Such an inference is coherent with natural examples and analogue models of multiphase rift systems, where it is commonly observed that oblique inherited structures can be reactivated synchronously with the formation of new faults oriented perpendicular to the stretching direction (e.g. McClay and White, 1995; Mart and Dauteuil, 2000; Henza et al., 2010; Brune et al., 2014; Naliboff and Buiter, 2015; Zwaan et al., 2016; Zwaan and Schreurs, 2017; Cadenas et al., 2020). An alternative

hypothesis is that the lozenge-shaped structures are pull-apart basins or ridges associated with transtensive/transpressive faults. We discard this hypothesis for the studied area, as we do not observe the diagnostic features of wrench tectonics, such as positive/negative flowers, branch faults, restraining/releasing bends, antithetic faults and/or strike-slip duplexes (e.g. Riedel, 1929; Wilcox et al., 1973; Harding, 1974; Aydin and Nur, 1982; Sanderson and Marchini, 1984; Woodcock and Fischer, 1986; Sylvester, 1988; among others) in the L3NAM2012AR ~~seismic~~ 3D seismic cube~~dataset~~. Similarly to megasequences 7 and 6, megasequence 5 thickens towards the NE (Fig. 7e), suggesting that these megasequences form part of the same multiphase rift system.

After diminishing the rifting-related Jurassic crustal extensions (e.g. Ziegler, 1992), the WNB entered a post-rift phase by the Early Cretaceous (van Wijhe, 1987), during which megasequence 4 deposited. None of the observed extensional faults were active at that time. Post-rift infill of the WNB is well represented by megasequence 4 on the flattened displays of ~~sections~~diplines 2610, ~~and~~ 3410 and 4225 (~~F~~Figs. 3c~~b~~, ~~&~~ 4c~~b~~ and 5c) and on the thickness map, showing a NW-SE elongated, 20 to 40 km wide, post-rift basin where the thickness of megasequence 4 increases with roughly 1000 m (Fig. 7d). Such a broad basin does not overlap the syn-rift grabens and, therefore, it likely relates to large-scale sagging rather than to the simple passive infill of the previously developed half-grabens.

On top of the post-rift megasequence 4, the Lower Cretaceous megasequence 3 was deposited during a shortening stage. Positively inverted normal faults with associated growth geometries and buttressing-related structures are observed in this megasequence (e.g. associated with faults *e*, *h* and *i* in Fig. 3 and fault *a* in Fig. 5). This Late Cretaceous period of inversion likely corresponds to the Late Cretaceous Subhercynian inversion phase (Fig. 2) (e.g. Ziegler, 1992; van Wijhe, 1987; de Jager 2003, Worum and Michon, 2005), caused by the convergence between Africa and Europa (Kley and Voigt, 2008). During this stage, both faults of the NW-SE and NNW-SSE systems have been inverted or deformed during buttressing. Yet, we were not able to individuate newly formed reverse faults, which are needed to constrain the shortening direction. While the NE-section of the WNB got inverted and uplifted, its SW-flank became subject to subsidence and developed into a marginal basin, referred to as the Voorne Trough (Deckers, 2015) and well-illustrated by the thickness increase of megasequence 3 from 0 m in the NE to 800 m in the SW~~-ward thickness increase of megasequence 3~~ (Fig. 7c). The upper portion of megasequence 3 could already include a post-inversion succession. In fact, a local unconformity divides the upper from the central and lower portions of this megasequence, as illustrated in figures 3, 4 and 5 by a black dotted line. This is consistent with regional constraints, indicating that due to a decrease in convergence rate between Africa and Europa (Rosenbaum et al., 2002), the Subhercynian inversion ceased after the Campanian (de Jager, 2003), whereafter deposition of the chalk of megasequence 3 continued for the entire Late Cretaceous (van Balen et al., 2000; van der Voet et al., 2019).

Megasequence 2 is separated from the underlying megasequence 3 by a regional unconformity. No growth wedge geometries are observed in this megasequence, suggesting that the gentle folding of its base is associated with compaction of the underlying sediments and/or the passive infill/draping of a paleo-topography. Both syn-inversion megasequence 3 and post-inversion megasequence 2 thin out toward the NE (Figs. 7b and 7c), indicating that uplift of the NE sector of the study area started during faults' inversion but continued during the deposition of megasequence 2, as also evidenced by the SW-tilting of

the erosional unconformity separating the two megasequences. The erosional unconformity at the base of megasequence 2 likely corresponds to the timing of the Laramide uplift that peaked during the Middle Paleocene (Deckers, 2015), which may be related to a significant drop in global sea-level (Haq et al., 1987), along with a contribution from dynamic topography associated with mantle flow (Kley, 2018; Voigt et al., 2021). The Laramide tectonic phase is believed to have caused basin uplift in the area of the WNB (Deckers and van der Voet, 2018; Kley, 2018). The erosional unconformity at the top of megasequence 2, instead, reflects the broad basin uplift (de Jager, 2003), likely initiated by the Alpine Orogeny (Worum and Michon, 2005). Lastly, the depth map of the base of megasequence 1 displays two large plateaus, separated by an ENE-dipping fault formed during the second extensional phase and reactivated during these times.

5.2 Implications for geothermal systems

The WNB harbours well developed geothermal reservoir rocks and is covered by a good data-collection, inherited from former hydrocarbon exploration. Presently, the most exploited geothermal reservoir units are the Late Jurassic Nieuwerkerk Formation (megasequence 5; second syn-rift) and, subordinately, the Cretaceous sandstones (megasequence 4, post-rift and pre-inversion). An additional reservoir is represented by the Triassic sandstones, which occur at deeper structural levels, and have not been mapped in this work. Yet, although the observed first rifting period is Early Jurassic in age, ~~its rifting architecture~~ the rift-related structures might be applicable to the Triassic reservoir as well. This Early Jurassic rifting episode can be linked to the regional Early Kimmerian tectonic phase, which started during the early Late Triassic (e.g. van Wijhe, 1987; Ziegler, 1992; Geluk and Röhling, 1997, Fig. 2) and reactivated basement faults (Kortekaas et al., 2018), wherefore the Early Jurassic rift might be a remnant from Triassic tectonics. ~~Rift initiation already happened during the Triassic (e.g. Ziegler, 1992; van Wijhe, 1987), wherefore the Early Jurassic rift possibly is a remnant from Triassic extensional tectonics. Although t~~The Triassic sandstones are known for having a reduced reservoir quality (Boersma et al., 2020). However, ~~underneath the Zoetermeer High (structure XV in figs. 3b and 7h) the reservoir quality might be better. Here,~~ the Zoetermeer High (structure XV in figures 3b and 7h) ~~structural high~~ seems to have been relatively stable throughout the evolution of the ~~basin~~WNB, as evidenced by the fault *k* that does not show~~ing no~~ signs of reactivation during inversion (Fig. 3). Therefore, the Triassic reservoir might be less fractured, with shallower burial conditions than in the surrounding grabens, and its quality as geothermal reservoir may be better.

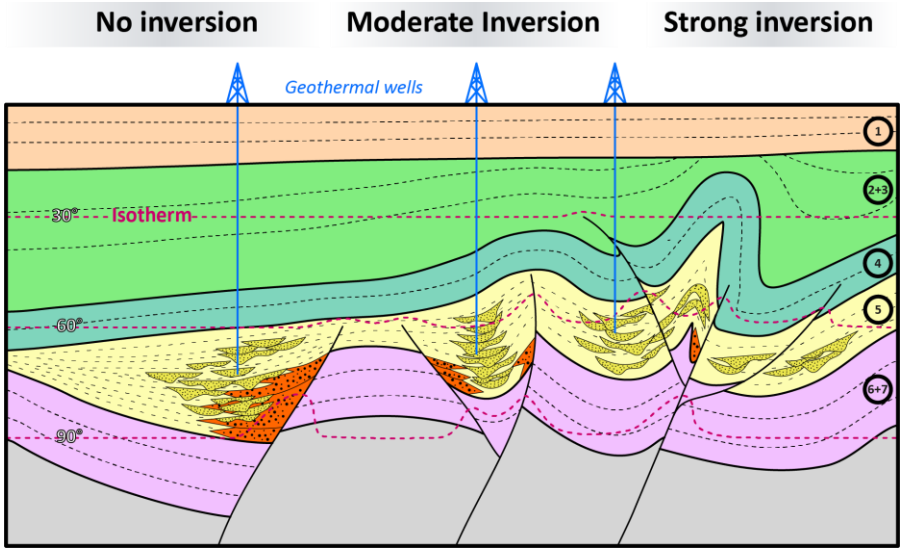

Figure 8: Simplified ~~figure~~cartoon, showing the geothermal play of a fluvial-deltaic reservoir in an inverted rift basin. The expected best spots for geothermal exploration are the central portions of the ~~growth synclines~~half-grabens, where the fluvial sands (yellow dotted material) are present, the geothermal gradients are highest, and the interference from foot-wall erosion (orange dotted material) is minor. The isotherms are based on a geotherm of 31°C km^{-1} (Bonté et al., 2012). The sketched layers ~~correspond to~~ are based on the interpreted megasequences o~~f~~n this study, indicated in the circles on the right side.

Among the two Jurassic-Cretaceous reservoirs, the Nieuwerkerk Formation is the most promising, facilitating a deeper reservoir (spanning in depth from 0.5 km to 3 km) and, given the geothermal gradient of the area (Fig. 8, 31°C km^{-1}; Bonté et al., 2012), likely offering temperatures up to 90°C, which is ~~perfect~~suitable for low enthalpy geothermal systems. Instead, temperatures for the Cretaceous sandstones probably do not exceed 60°C. The Nieuwerkerk Formation was deposited during the second rifting event in the Late Jurassic (megasequence 5) and the multi-phase extensional setting led to the development of a compartmentalised reservoir, made up of lozenge~~-~~shaped sub-basins. Given the fluvial nature of the Nieuwerkerk Formation (e.g. Willems et al., 2017c; Vondrak et al., 2018; Willems et al., 2020), the lateral and vertical compartmentalization of sands and shales is a characteristic that must be taken into account ~~in the~~for reservoir's geothermal exploration.

The geothermal play of such a fluvial-deltaic reservoir in an inverted rift basin is illustrated in Figure 8, where normal faults, positively inverted normal faults, half-grabens, geotherms and sweet spots are outlined. In rift systems involving continental to coastal clastic syn-tectonic sedimentation, it is well known that the more coarse~~-~~grained facies are located close to the faults and along the axis of grabens and half-grabens (e.g., Gawthorpe and Leeder, 2000). In agreement, we expect the fluvial channels and other coarse grained sediments to be located in the core of half-grabens or in their inner limb (i.e. the limb close to the master fault). Furthermore, close to the master fault, foot-wall erosion and related hanging-wall degradation complexes

drive the development of a wide spectrum of heterogeneous sedimentary facies, possibly interfingering with the targeted reservoir rock. In contrast ~~Contrasting~~ to petroleum systems, in which structural highs are the preferential target for hydrocarbon exploration (hydrocarbons are lighter than water) (e.g. Bjørlykke, 2010), half-grabens are the most suitable sites for geothermal exploration. Indeed, half-grabens are found at deeper levels, thus ensuring higher temperatures with respect to limbs and structural highs. ~~Combining all that is stated above~~ All these characteristics allows us to individuate the core of half-grabens, i.e. syn-tectonic intervals in the core of half-grabens, as preferential sites for geothermal exploration. ~~Here, t~~The chances of finding hot and thick fluvial sand packages with a higher nett to gross ratio, are higher~~increased~~.

Such a simple template is modified during faults' reactivation and buttressing associated with ~~the~~ inversion ~~stage~~tectonics. Such an inversion can produce (1) the uplift of the former structural-stratigraphic reservoirs, i.e. the half-grabens, with the consequent decrease of water temperatures and, eventually, (2) fracturing of the reservoirs by second order faults and brecciation and breaching of the reservoir ~~when the amount of~~ due to an increase in the inversion ~~increases~~ (e.g. Tari et al., 2020). ~~All the above discussed features are schematically illustrated in Figure 8, where normal faults, positively inverted normal faults, half-grabens, geotherms, and sweet spots are outlined.~~

Given the template illustrated in Figure 8 and assuming that the most suitable areas for geothermal exploration are the central portions of the half-grabens, ~~. S~~synclinal traps in half-grabens associated with strongly inverted faults are more likely to be breached by faults ~~developed~~ during inversion tectonics.

The effects of a secondary fracturing period due to inversion tectonics can be beneficial in terms of permeability (e.g. Fisher and Knipe, 2001). Instead, the consequences of breaching a geothermal reservoir due to inversion tectonics is less clear. In hydrocarbon reservoirs, indeed, breaching of the anticlinal traps has a clear negative effect (i.e. leakage of the hydrocarbons), while the consequences of breaching synclinal traps in geothermal systems are not yet fully understood. In order to de-risk geothermal exploitation, we therefore advise to choose half-grabens associated with either non-inverted or moderately inverted normal faults. By combining these findings, we can identify areas of interest for geothermal exploitation. Examples of such areas are the central portions of the Pijnacker, Rijswijk and Westland grabens (structures IV, VII and VIII, ~~f~~Figs. 4, 7e and 7h). Here, the grabens contain a 1 km to 1,4 km thick ~~(1 to 1,4 km in thickness)~~ megasequence 5 ~~package of~~ (Nieuwerkerk Formation) with ~~, while displaying~~ no to moderate inversion. The deepest portions of these grabens are located away from the master fault, preventing interference by material originating from foot-wall erosion (e.g. the Pijnacker Graben, structure IV, Fig. 4). The centres of these grabens are located at depths roughly between 2 and 3 km (Fig. 4b), giving the present sand bodies expected temperatures between 60°C and 90°C (based on a geotherm of 31°C km^{-1}; Bonté et al., 2012). In such areas, additional work is required to assess the fluvial reservoir architecture (Willems et al., 2017a) in more detail and properly locate injection and recovery wells (i.e. geothermal doublets) within coarse grained sediments.

6 ~~6~~ Conclusion

The ~~A renewed~~ seismic interpretation of the recently released L3NAM2012AR ~~seismic~~ 3D depth-migrated seismic ~~dataset~~cube~~,~~ allowed for the identification of seven megasequences and three main sets of faults, and the mapping of horst and grabens and major bounding faults in the ~~a detailed study of the sub-seismic structural geology of the~~ WNB. This ~~, which~~ helps to better understand the regional structure of the sedimentary aquifer architecture, the fault activation and reactivation, and the development of the syn-rift infill.~~.~~

- The fault activation and reactivation, together with the development of its syn-rift infill, can be described as a series of tectonic events. ~~were re-assessed.~~Faults affecting the Mesozoic sequence of the WNB are arranged in three sets. A first set of reverse faults affect the basins' infill up to Cretaceous strata and include faults reversely reactivated during basin inversion. The second set includes extensional faults that cut through the sediments up to the Late Jurassic (megasequence 5) and developed during Late Jurassic rifting. The third set includes extensional faults developed or reactivated during Early Jurassic extension, that later became reactivated during Late Jurassic rifting.
- Together with the above described observations, ~~From Jurassic times onwards,~~ seven main phases~~megasequences could be~~were documented from Jurassic times onwards; (1): ~~: (1) a~~a first NE-SW oriented rifting phase during the Early Jurassic; (2): ~~; (2) a~~ a post-rift phase during the Middle Jurassic; (3): ~~; (3): a~~a second WSW-ENE oriented rifting phase during the Late Jurassic, partly controlled by the Early Jurassic rifting phase; (4): a~~; (4): a~~n Early Cretaceous post-rift sag phase; (5): ~~; (5): f~~faults' inversion during the Late Cretaceous; (6): b~~; (6): b~~road basin uplift during the Paleocene to Oligocene; (7):~~; (7): a~~ a minor reactivation event during the Miocene.
-
- The lozenge-shaped sub-basins of megasequence 5 show that~~M~~ multi-phase rifting during the Jurassic led to compartmentalization of the ~~second syn-rift infill, which is the~~ main geothermal target in the WNB; the Late Jurassic fluvial-deltaic Nieuwerkerk Formation.
- The presence of heterogeneous seismic facies within the syn-rift infill of the Nieuwerkerk Formation in the half-graben structures suggest that channel sands are likely present in the deepest, central portions of the half-graben structures. ~~We expect its channel sands to be present in the deepest, central portions of the half-grabens, H~~where, the highest temperatures are expected and~~. Here,~~ interference by foot-wall erosion and residue hydrocarbons is expected to be minor.
- The Late Cretaceous inversion needs to be taken into account, as an increasing amount of inversion can form risks for geothermal exploration. Reactivation of the faults~~, as it~~ could have caused breaching of the reservoir and uplift of the targeted half-grabens, hence lowering the temperature. Therefore, only non to moderately inverted areas should be considered for geothermal exploration.

Met opmaak: Genummerd + Niveau: 1 + Nummeringstijl: 1, 2, 3, … + Beginnen bij: 6 + Uitlijning: Links + Uitgelijnd op: 0.63 cm + Inspringen op: 1.27 cm

Met opmaak: Lijstalinea, Met opsommingstekens + Niveau: 1 + Uitgelijnd op: 0.63 cm + Inspringen op: 1.27 cm

Met opmaak: Lijstalinea, Met opsommingstekens + Niveau: 1 + Uitgelijnd op: 0.63 cm + Inspringen op: 1.27 cm

Hence, we conclude that for a geothermal play in a multi-phase rift setting with subsequent basin inversion and a fluvial-deltaic syn-rift reservoir rock, the best spots for geothermal exploration can be found in the central portions of non to moderately inverted half-grabens.

Supplementary materials

The supplementary materials include:~~;~~

- a list of used wells with their coordinates, drilling result and whether a LAS-file is available,~~,~~
- links to the public datasets with a description of how to download them,
- ~~and~~ a folder with TIFF-files of~~with~~ the uninterpreted seismic lines together with some information about the L3NAM2012AR 3D seismic cube and how to download it.~~ can be found with this article.~~

Met opmaak: Lijstalinea, Met opsommingstekens + Niveau: 1 + Uitgelijnd op: 0.63 cm + Inspringen op: 1.27 cm

Author contribution

AW, corresponding author, conceptualisation, data acquisition and processing, seismic interpretation, figures and manuscript drafting/editing; KO, interpretation assistance, figures and manuscript drafting/editing; FV, data acquisition, manuscript drafting/editing; CL, data acquisition, interpretation assistance, manuscript drafting/editing; GB, manuscript drafting/editing; JA, manuscript drafting/editing; ST, conceptualisation, data processing, interpretation assistance, figures and manuscript drafting/editing.

Competing interests

KO and ST are member of the editorial board of Solid Earth.

Acknowledgments

This work was funded by a full PhD scholarship (PON-REACTEU) from the Ministry of University and Research of Italy. PanTerra Geoconsultants B.V. is thanked for funding this project and for providing in-house expertise that greatly improved the quality of the research. We thank Schlumberger for providing access to Petrel Software (version 2020.3). David Iacopini is thanked for his help that greatly improved the quality of the work. We thank an anonymous reviewer and Connor O'Sullivan for their detailed and constructive comments and suggestions, which allowed us to improve the manuscript. The handling editor Patricia Cadenas Martínez and the executive editor Susanne Buiter are also thanked for guiding the review process.

References

van Adrichem Boogaert, H. A. and Kouwe, W. P. F.: Stratigraphic nomenclature of the Netherlands, revision and update by RGD and NOGEPA, 1993.

Aydin, A. and Nur, A.: Evolution of pull-apart basins and their scale independence, Tectonics, 1, 91–105, https://doi.org/10.1029/TC001i001p00091, 1982.

van Balen, R. T., van Bergen, F., de Leeuw, C., Pagnier, H., Simmelink, H., van Wees, J. D., and Verweij, J. M.: Modelling the hydrocarbon generation and migration in the West Netherlands Basin, the Netherlands, Netherlands Journal of Geosciences - Geologie en Mijnbouw, 79, 29–44, https://doi.org/10.1017/S0016774600021557, 2000.

Bjørlykke, K. (Ed.): Petroleum Geoscience: From sedimentary environments to rock physics, Springer Science and Business Media, Heidelberg, Germany, 662 pp., ISBN 978-3-642-34131-1, 2010.

Boersma, Q. D., Bruna, P. O., de Hoop, S., Vinci, F., Moradi Tehrani, A., and Bertotti, G.: The impact of natural fractures on heat extraction from tight Triassic sandstones in the West Netherlands Basin: a case study combining well, seismic and numerical data, Netherlands Journal of Geosciences, 100, e6, https://doi.org/10.1017/njg.2020.21, 2021.

Bonté, D., van Wees, J. D., and Verweij, J. M.: Subsurface temperature of the onshore Netherlands: new temperature dataset and modelling, Netherlands Journal of Geosciences - Geologie en Mijnbouw, 91, 491–515, https://doi.org/10.1017/S0016774600000354, 2012.

Brune, S., Heine, C., Pérez-Gussinyé, M., and Sobolev, S. V.: Rift migration explains continental margin asymmetry and crustal hyper-extension, Nat Commun, 5, 4014, https://doi.org/10.1038/ncomms5014, 2014.

Cadenas, P., Manatschal, G., and Fernández-Viejo, G.: Unravelling the architecture and evolution of the inverted multi-stage North Iberian-Bay of Biscay rift, Gondwana Research, 88, 67-87, https://doi.org/10.1016/j.gr.2020.06.026, 2020.

Carapezza, M. L., Chiappini, M., Nicolosi, I., Pizzino, L., Ranaldi, M., Tarchini, L., de Simone, G., Ricchetti, N., and Barberi, F.: Assessment of a low-enthalpy geothermal resource and evaluation of the natural CO2 output in the Tor di Quinto area (Rome city, Italy), Geothermics, 99, 102298, https://doi.org/10.1016/j.geothermics.2021.102298, 2022.

Gewijzigde veldcode

heeft opmaak toegepast: Engels (Verenigd Koninkrijk)

heeft opmaak toegepast: Engels (Verenigd Koninkrijk)

Crooijmans, R. A., Willems, C. J. L., Nick, H. M., and Bruhn, D. F.: The influence of facies heterogeneity on the doublet performance in low-enthalpy geothermal sedimentary reservoirs, Geothermics, 64, 209–219, https://doi.org/10.1016/j.geothermics.2016.06.004, 2016.

Deckers, J.: The Paleocene stratigraphic records in the Central Netherlands and close surrounding basins: Highlighting the different responses to a late Danian change in stress regime within the Central European Basin System, Tectonophysics, 659, 102–108, https://doi.org/10.1016/j.tecto.2015.07.031, 2015.

Deckers, J. and van der Voet, E.: A review on the structural styles of deformation during Late Cretaceous and Paleocene tectonic phases in the southern North Sea area, J Geodyn, 115, 1–9, https://doi.org/10.1016/j.jog.2018.01.005, 2018.

DeVault, B. and Jeremiah, J.: Tectonostratigraphy of the Nieuwerkerk Formation (Delfland subgroup), West Netherlands Basin, AAPG bulletin, 86, 1679-1707, https://doi.org/10.1306/61EEDD50-173E-11D7-8645000102C1865D, 2002.

Duin, E. J. T., Doornenbal, J. C., Rijkers, R. H. B., Verbeek, J. W., and Wong, Th. E.: Subsurface structure of the Netherlands - results of recent onshore and offshore mapping, Netherlands Journal of Geosciences - Geologie en Mijnbouw, 85, 245–276, https://doi.org/10.1017/S0016774600023064, 2006.

Færseth, R. B.: Interaction of Permo-Triassic and Jurassic extensional fault-blocks during the development of the northern North Sea, J Geol Soc London, 153, 931–944, https://doi.org/10.1144/gsjgs.153.6.0931, 1996.

Fisher, Q. J. and Knipe, R. J.: The permeability of faults within siliciclastic petroleum reservoirs of the North Sea and Norwegian Continental Shelf, Marine and Petroleum Geology, 18, 1063–1081, https://doi.org/10.1016/S0264-8172(01)00042-3, 2001.

Fossen, H., Ksienzyk, A. K., Rotevatn, A., Bauck, M. S., and Wemmer, K.: From widespread faulting to localised rifting: Evidence from K-Ar fault gouge dates from the Norwegian North Sea rift shoulder, Basin Research, 33, 1934–1953, https://doi.org/10.1111/bre.12541, 2021.

Franke, D.: Rifting, lithosphere breakup and volcanism: Comparison of magma-poor and volcanic rifted margins, Mar Pet Geol, 43, 63–87, https://doi.org/10.1016/j.marpetgeo.2012.11.003, 2013.

Gawthorpe, R. L. and Leeder, M. R.: Tectono-sedimentary evolution of active extensional basins, Basin Research, 12, 195–218, https://doi.org/10.1111/j.1365-2117.2000.00121.x, 2000.

Geluk, M. C. and Röhling, H. G.: High-resolution sequence stratigraphy of the Lower Triassic Buntsandstein in the Netherlands and Northwestern Germany, Geologie en Mijnbouw (Geology and Mining), 76, 227–246, https://doi.org/10.1023/A:1003062521373, 1997.

Geluk, M. C., Plomp, A., and van Doorn, T. H. M.: Development of the Permo-Triassic succession in the basin fringe area, southern Netherlands, in: Geology of Gas and Oil under the Netherlands, Springer Netherlands, Dordrecht, 57–78, https://doi.org/10.1007/978-94-009-0121-6_7, 1996.

Geothermie Nederland: Locaties op de kaart, https://geothermie.nl/geothermie/locaties-op-kaart/, last access: 25 May 2023.

Gouiza, M. and Paton, D. A.: The Role of Inherited Lithospheric Heterogeneities in Defining the Crustal Architecture of Rifted Margins and the Magmatic Budget During Continental Breakup, Geochemistry, Geophysics, Geosystems, 20, 1836–1853, https://doi.org/10.1029/2018GC007808, 2019.

Harding, T. P.: Petroleum Traps Associated with Wrench Faults, Am Assoc Pet Geol Bull, 58, https://doi.org/10.1306/83D91669-16C7-11D7-8645000102C1865D, 1974.

den Hartog Jager, D. G.: Fluviomarine sequences in the Lower Cretaceous of the West Netherlands Basin: correlation and seismic expression, in: Geology of Gas and Oil under the Netherlands, Springer Netherlands, Dordrecht, 229–241, https://doi.org/10.1007/978-94-009-0121-6_19, 1996.

Haq, B. U., Hardenbol, J., and Vail, P. R.: Chronology of fluctuating sea levels since the Triassic, Science, 235, 1156-1167, https://doi.org/10.1126/science.235.4793.1156, 1987.

Henstra, G. A., Berg Kristensen, T., Rotevatn, A., and Gawthorpe, R. L.: How do pre-existing normal faults influence rift geometry? A comparison of adjacent basins with contrasting underlying structure on the Lofoten Margin, Norway, Basin Research, 31, 1083–1097, https://doi.org/10.1111/bre.12358, 2019.

Henza, A. A., Withjack, M. O., and Schlische, R. W.: Normal-fault development during two phases of non-coaxial extension: An experimental study, J Struct Geol, 32, 1656–1667, https://doi.org/10.1016/j.jsg.2009.07.007, 2010.

Gewijzigde veldcode

Herngreen, G. F. W., Kouwe, W. F. P., and Wong, T. E.: The Jurassic of the Netherlands, Geological Survey of Denmark and Greenland Bulletin, 1, 217–230, https://doi.org/10.34194/geusb.v1.4652, 2003.

de Jager, J., Doyle, M. A., Grantham, P. J., and Mabillard, J. E.: Hydrocarbon habitat of the West Netherlands Basin, in: Geology of Gas and Oil under the Netherlands, Springer Netherlands, Dordrecht, 191–209, https://doi.org/10.1007/978-94-009-0121-6_17, 1996.

de Jager, J.: Inverted basins in the Netherlands, similarities and differences, Netherlands Journal of Geosciences - Geologie en Mijnbouw, 82, 339–349, https://doi.org/10.1017/S0016774600020175, 2003.

Jeremiah, J. M., Duxbury, S., and Rawson, P.: Lower Cretaceous of the southern North Sea Basins: reservoir distribution within a sequence stratigraphic framework, Netherlands Journal of Geosciences - Geologie en Mijnbouw, 89, 203–237, https://doi.org/10.1017/S0016774600000706, 2010.

Kley, J.: Timing and spatial patterns of Cretaceous and Cenozoic inversion in the Southern Permian Basin, Geological Society, London, Special Publications, 469, 19–31, https://doi.org/10.1144/SP469.12, 2018.

Kley, J. and Voigt, T.: Late Cretaceous intraplate thrusting in central Europe: Effect of Africa-Iberia-Europe convergence, not Alpine collision, Geology, 36, 839-842, https://doi.org/10.1130/G24930A.1, 2008.

Kramers, L., van Wees, J. D., Pluymaekers, M. P. D., Kronimus, A., and Boxem, T.: Direct heat resource assessment and subsurface information systems for geothermal aquifers; the Dutch perspective, Netherlands Journal of Geosciences - Geologie en Mijnbouw, 91, 637–649, https://doi.org/10.1017/S0016774600000421, 2012.

Kombrink, H., Doornenbal, J. C., Duin, E. J. T., den Dulk, M., ten Veen, J. H., and Witmans, N.: New insights into the geological structure of the Netherlands; results of a detailed mapping project, Netherlands Journal of Geosciences - Geologie en Mijnbouw, 91, 419–446, https://doi.org/10.1017/S0016774600000329, 2012.

Kortekaas, M., Böker, U., van der Kooij, C., and Jaarsma, B.: Lower Triassic reservoir development in the northern Dutch offshore, Geological Society, London, Special Publications, 469, 149-168, https://doi.org/10.1144/SP469.19, 2018.

Limberger, J., Boxem, T., Pluymaekers, M., Bruhn, D., Manzella, A., Calcagno, P., Beekman, F., Cloetingh, S., and van Wees, J. D. (2018). Geothermal energy in deep aquifers: A global assessment of the resource base for direct heat utilization, Renewable and Sustainable Energy Reviews, 82, 961-975, https://doi.org/10.1016/j.rser.2017.09.084, 2018.

heeft opmaak toegepast: Engels (Verenigd Koninkrijk)

heeft opmaak toegepast: Engels (Verenigd Koninkrijk)

Mart, Y. and Dauteuil, O.: Analogue experiments of propagation of oblique rifts, Tectonophysics, 316, 121–132, https://doi.org/10.1016/S0040-1951(99)00231-0, 2000.

McClay, K. R. and White, M. J.: Analogue modelling of orthogonal and oblique rifting, Mar Pet Geol, 12, 137–151, https://doi.org/10.1016/0264-8172(95)92835-K, 1995.

Michon, L., van Balen, R. T., Merle, O., and Pagnier, H.: The Cenozoic evolution of the Roer Valley Rift System integrated at a European scale, Tectonophysics, 367, 101–126, https://doi.org/10.1016/S0040-1951(03)00132-X, 2003.

Mijnlieff, H. F.: Introduction to the geothermal play and reservoir geology of the Netherlands, Netherlands Journal of Geosciences, 99, e2, https://doi.org/10.1017/njg.2020.2, 2020.

Naliboff, J. and Buiter, S. J. H.: Rift reactivation and migration during multiphase extension, Earth Planet Sci Lett, 421, 58–67, https://doi.org/10.1016/j.epsl.2015.03.050, 2015.

O'Sullivan, C. M., Childs, C. J., Saqab, M. M., Walsh, J. J., and Shannon, P. M.: Tectonostratigraphic evolution of the Slyne Basin, Solid Earth, 13, 1649–1671, https://doi.org/10.5194/se-13-1649-2022, 2022.

Peron-Pinvidic, G. and Manatschal, G.: Rifted Margins: State of the Art and Future Challenges, Front Earth Sci (Lausanne), 7, https://doi.org/10.3389/feart.2019.00218, 2019.

Poulsen, S. E., Balling, N., and Nielsen, S. B.: A parametric study of the thermal recharge of low enthalpy geothermal reservoirs, Geothermics, 53, 464–478, https://doi.org/10.1016/j.geothermics.2014.08.003, 2015.

Racero-Baena, A. and Drake, S. J.: Structural style and reservoir development in the West Netherlands oil province, in: Geology of Gas and Oil under the Netherlands, Springer Netherlands, Dordrecht, 211–227, https://doi.org/10.1007/978-94-009-0121-6_18, 1996.

Riedel, W.: Zur Mechanik geologischer Brucherscheinungen ein Beitrag zum Problem der Fiederspatten, Centralblatt für Mineralogie, Geologie und Paläontologie, 354-368,1929.

Rosenbaum, G., Lister, G. S., and Duboz, C.: Relative motions of Africa, Iberia and Europe during Alpine orogeny, Tectonophysics, 359, 117-129, https://doi.org/10.1016/S0040-1951(02)00442-0, 2002.

Sanderson, D. J. and Marchini, W. R. D.: Transpression, J Struct Geol, 6, 449–458, https://doi.org/10.1016/0191-8141(84)90058-0, 1984.

Sissingh, W.: Palaeozoic and Mesozoic igneous activity in the Netherlands: a tectonomagmatic review, Netherlands Journal of Geosciences - Geologie en Mijnbouw, 83, 113–134, https://doi.org/10.1017/S0016774600020084, 2004.

Sylvester, A. G.: Strike-slip faults, Geol Soc Am Bull, 100, 1666–1703, https://doi.org/10.1130/0016-7606(1988)100%3C1666:SSF%3E2.3.CO;2, 1988.

Tari, G., Arbouille, D., Schléder, Z., and Tóth, T.: Inversion tectonics: a brief petroleum industry perspective, Solid Earth, 11, 1865-1889, https://doi.org/10.5194/se-11-1865-2020, 2020.

TNO-GDN: Stratigraphic Nomenclature of the Netherlands, https://www.dinoloket.nl/en/stratigraphic-nomenclature, last access: 10 May 2023.

van der Voet, E., Heijnen, L., and Reijmer, J. J. G.: Geological evolution of the Chalk Group in the northern Dutch North Sea: inversion, sedimentation and redeposition, Geol Mag, 156, 1265–1284, https://doi.org/10.1017/S0016756818000572, 2019.

Voigt, T., Kley, J., and Voigt, S.: Dawn and dusk of Late Cretaceous basin inversion in central Europe, Solid Earth, 12, 1443-1471, https://doi.org/10.5194/se-12-1443-2021, 2021.

Vondrak, A. G., Donselaar, M. E., and Munsterman, D. K.: Reservoir architecture model of the Nieuwerkerk Formation (Early Cretaceous, West Netherlands Basin): diachronous development of sand-prone fluvial deposits, Geological Society, London, Special Publications, 469, 423–434, https://doi.org/10.1144/SP469.18, 2018.

van Wijhe, D. H.: Structural evolution of inverted basins in the Dutch offshore, Tectonophysics, 137, 171–219, https://doi.org/10.1016/0040-1951(87)90320-9, 1987.

Wilcox, R. E., Harding, T. P., and Seely D. R.: Basic Wrench Tectonics, AAPG Bulletin, 57, 74-96, 1973.

Willems, C. J. L.: Doublet deployment strategies for geothermal Hot Sedimentary Aquifer exploitation: Application to the Lower Cretaceous Nieuwerkerk Formation in the West Netherlands Basin, Delft University of Technology, The Netherlands, 147 pp., 2017.

Willems, C. J. L. and M. Nick, H.: Towards optimisation of geothermal heat recovery: An example from the West Netherlands Basin, Appl Energy, 247, 582–593, https://doi.org/10.1016/j.apenergy.2019.04.083, 2019.

Willems, C. J. L., Nick, H. M., Donselaar, M. E., Weltje, G. J., and Bruhn, D. F.: On the connectivity anisotropy in fluvial Hot Sedimentary Aquifers and its influence on geothermal doublet performance, Geothermics, 65, 222–233, https://doi.org/10.1016/j.geothermics.2016.10.002, 2017a.

Willems, C. J. L., Nick, H. M., Weltje, G. J., and Bruhn, D. F.: An evaluation of interferences in heat production from low enthalpy geothermal doublets systems, Energy, 135, 500-512, https://doi.org/10.1016/j.energy.2017.06.129, 2017b.

Willems, C. J. L., Vondrak, A., Munsterman, D. K., Donselaar, M. E., and Mijnlieff, H. F.: Regional geothermal aquifer architecture of the fluvial Lower Cretaceous Nieuwerkerk Formation – a palynological analysis, Netherlands Journal of Geosciences, 96, 319–330, https://doi.org/10.1017/njg.2017.23, 2017c.

Willems, C. J. L., Vondrak, A., Mijnlieff, H. F., Donselaar, M. E., and van Kempen, B. M. M.: Geology of the Upper Jurassic to Lower Cretaceous geothermal aquifers in the West Netherlands Basin – an overview, Netherlands Journal of Geosciences, 99, e1, https://doi.org/10.1017/njg.2020.1, 2020.

Williams, G. D., Powell, C. M., and Cooper, M. A.: Geometry and kinematics of inversion tectonics, Geological Society, London, Special Publications, 44, 3–15, https://doi.org/10.1144/GSL.SP.1989.044.01.02, 1989.

Wong, T. E, Batjes, D. A. J., and de Jager, J. (Eds.): Geology of the Netherlands, Royal Netherlands Academy of Arts and Sciences, Amsterdam, The Netherlands, 362 pp., ISBN 978-9069844817, 2007.

Woodcock, N. H. and Fischer, M.: Strike-slip duplexes, J Struct Geol, 8, 725–735, https://doi.org/10.1016/0191-8141(86)90021-0, 1986.

Worum, G. and Michon, L.: Implications of continuous structural inversion in the West Netherlands Basin for understanding controls on Palaeogene deformation in NW Europe, J Geol Soc London, 162, 73–85, https://doi.org/10.1144/0016-764904-011, 2005.

Worum, G., Michon, L., van Balen, R., van Wees, J., Cloetingh, S., and Pagnier, H.: Pre-Neogene controls on present-day fault activity in the West Netherlands Basin and Roer Valley Rift System (southern Netherlands): role of variations in fault orientation in a uniform low-stress regime, Quat Sci Rev, 24, 473–488, https://doi.org/10.1016/j.quascirev.2004.02.020, 2005.

Ziegler, P. A.: North Sea rift system, Tectonophysics, 208, 55–75, https://doi.org/10.1016/0040-1951(92)90336-5, 1992.

Zwaan, F. and Schreurs, G.: How oblique extension and structural inheritance influence rift segment interaction: Insights from 4D analog models, Interpretation, 5, SD119–SD138, https://doi.org/10.1190/INT-2016-0063.1, 2017.

Zwaan, F., Schreurs, G., Naliboff, J., and Buiter, S. J. H.: Insights into the effects of oblique extension on continental rift interaction from 3D analogue and numerical models, Tectonophysics, 693, 239–260, https://doi.org/10.1016/j.tecto.2016.02.036, 2016.